Heterosynaptic Plasticity of the Visuo-auditory Projection Requires Cholecystokinin released from Entorhinal Cortex Afferents

Wenjian Sun [1,2,6,†], Haohao Wu[3,7,8†], Yujie Peng [1,2,9,†], Peng Tang [1,2], Ming Zhao[3], Xuejiao Zheng[1,2], Hemin Feng [1,2,10], Hao Li [1,2], Ye Liang [1,2], Jing Li [1,2], Junfeng Su[1,11], Xi Chen[1,4,*], Tomas Hökfelt[3,5,*], Jufang He[1,4,*]

Affiliations

[1]Department of Neuroscience, City University of Hong Kong, Kowloon Tong, Hong Kong SAR, P.R. China, 0000

[2]Centre for Regenerative Medicine and Health, Hong Kong Institute of Science & Innovation, Chinese Academy of Sciences, Hong Kong SAR, P.R. China, 0000

[3]Department of Neuroscience, Karolinska Institutet, Stockholm, Sweden, 17177

[4]City University of Hong Kong Shenzhen Research Institute, Shenzhen, China, 518507

[5]Institute of Advanced Study, City University of Hong Kong, Kowloon Tong, Hong Kong SAR, P.R. China, 0000

[6]Current address: Zilkha Neurogenetic Institute, University of Southern California, Los Angeles, CA, USA, 90033

[7]Current address: Biozentrum, Department of Cell Biology, University of Basel, Basel, Switzerland, CH-4046

[8]Current address: Friedrich Miescher Institute for Biomedical Research, Basel, Switzerland, CH-4058

[9]Current address: Beijing Genomics Institute-Shenzhen, Shenzhen, China, 518103

[10]Current address: Department of Neurosurgery, Stanford University School of Medicine, Stanford, CA, USA, 94305

[11]Current address: F.M. Kirby Neurobiology Center, Boston Children's Hospital, Boston, MA，USA, 02115

[†]Equal Contributions

*Corresponding Authors: Jufang He, jufanghe@cityu.edu.hk; Tomas Hökfelt, tomas.hokfelt@ki.se; Xi Chen, xi.chen@um.cityu.edu.hk

Abstract

The entorhinal cortex is involved in establishing enduring visuo-auditory associative memory in the neocortex. Here we explored the mechanisms underlying this synaptic plasticity related to projections from the visual and entorhinal cortices to the auditory cortex, using optogenetics of dual pathways. High-frequency laser stimulation (HFLS) of the visuo-auditory projection did not induce long-term potentiation (LTP). However, after pairing with sound stimulus, the visuo-auditory inputs were potentiated following either infusion of cholecystokinin (CCK) or HFLS of the entorhino-auditory CCK-expressing projection. Combining retrograde tracing and RNAscope in situ hybridization, we show that CCK expression is higher in entorhinal cortex neurons projecting to the auditory cortex than in those originating from the visual cortex. In the presence of CCK, potentiation in the neocortex occurred when the pre-synaptic input arrived 200 ms before post-synaptic firing, even after just five trials of pairing. Behaviorally, inhibition of CCK signaling blocked the generation of associative memory. Our results indicate that neocortical visuo-auditory association is formed through heterosynaptic plasticity, which depends on release of CCK in the neocortex mostly from entorhinal afferents.

Key words

auditory cortex, cross-modal association, Hebbian plasticity, long-term potentiation, neuropeptides, optogenetics, pre- and post-synaptic coactivity, transmitter coexistence，visuo-auditory memory

Introduction

Cross-modal association is crucial for our brain to integrate information from different modalities to provide a useful output. Traditionally, this process is assumed to mainly occur in higher association cortices as evidenced by both anatomical(Cusick et al., 1995; Seltzer et al., 1996) and physiological(Fuster et al., 2000; Lipton et al., 1999; Sakai and Miyashita, 1991; Schlack et al., 2005; Sugihara et al., 2006) studies. Moreover, fMRI studies(Calvert et al., 1997; Finney et al., 2001; Foxe et al., 2002; Pekkola et al., 2006) and *in vivo* electrophysiological recordings(Brosch et al., 2005; Zhou and Fuster, 2004; Zhou and Fuster, 2000) have provided further evidence for involvement of unimodal sensory cortices. We have shown that neurons in the auditory cortex (AC) start to respond to light stimuli after classical fear conditioning, thus coupling light and electrical stimulation of the AC (ESAC) (Chen et al., 2013). These results indicate that the AC participates in the establishment of visuo-auditory association. However, the direct source of the visual signal to the AC is unclear. Here, we provide an anatomical foundation for a direct projection from the visual cortex (VC) to the AC by combining retrograde tracing and optogenetics in mice.

Observations of patient H.M. demonstrate that removal of the bilateral medial temporal lobe prevents the formation of long-term declarative memory(Milner and Klein, 2016; Scoville and Milner, 1957), suggesting that this lobe plays a crucial role in forming new memories about facts and events. The entorhinal cortex (EC) of the medial temporal lobe is strongly and reciprocally connected with both the neocortex and hippocampus(Canto et al., 2008; Swanson and Köhler, 1986).

It is well established that neocortex expresses a variety of neuropeptides, primarily in GABAergic, inhibitory interneurons (Hendry et al., 1984; Somogyi et al., 1984; Somogyi and Klausberger, 2005). The most abundant neuropeptide in brain is sulphated cholecystokinin octapeptide (CCK-8S) (Beinfeld et al., 1981; Dockray et al., 1978; Innis et al., 1979; Larsson and Rehfeld, 1979; Rehfeld, 1978; Vanderhaeghen et al., 1980), and this peptide was early shown to have excitatory effects on pyramidal neurons(Dodd and Kelly, 1981). CCK is, however, also found in pyramidal projection neurons, which have high levels of CCK transcript as shown with in situ hybridization (Burgunder and Young, 1988; Schiffmann and Vanderhaeghen, 1991; Siegel and Young, 1985). Several studies have reported that the EC is rich in CCK-positive $^{(+)}$

neurons, both in rat(Greenwood et al., 1981; Innis et al., 1979; Kohler and Chan-Palay, 1982) and mouse (Meziane et al., 1997). In fact, CCK plays an important role in learning and memory (Horinouchi et al., 2004; Lo et al., 2008; Meziane et al., 1993; Nomoto et al., 1999; Tsutsumi et al., 1999).

We have previously shown that the cortical projection neurons in the EC of mouse and rat mostly are CCK^+ and glutamatergic, and that this pathway is important for visuo-auditory association (Chen et al., 2019; Li et al., 2014; Zhang et al., 2020). Briefly, this type of association can be blocked by inactivation of the EC (Chen et al., 2013) or local infusion of a CCK-B receptor (CCKBR) antagonist(Li et al., 2014). Local infusion of a CCK agonist enabled visual responses in the auditory cortex after paring a light stimulus with a noise burst stimulus(Li et al., 2014). Moreover, we presented evidence that CCK released from the EC projection in the AC enables LTP and sound-sound association (Chen et al., 2019). Thus, the CCKBR antagonist blocked HFLS-induced neocortical LTP, and $CCK^{-/-}$ mice lacked such LTP (Chen et al., 2019). However, also an NMDAR antagonist blocked the LTP, a possible explanation being that CCK release is controlled by NMDA receptors (Chen et al., 2019).

In the present study we expanded our analysis of visuo-auditory association using two channelrhodopsins, Chronos and ChrimsonR, examining various ways to potentiate the responses to inputs/projection from VC to AC (VC→AC): (i) HFLS of VC→AC projection with classical high frequency stimulation protocol; (ii) infusion of a CCK agonist in the AC followed by pairing of presynaptic activation of VC→AC terminals expressing opsin by single pulse laser stimulation (SPLS) with postsynaptic noise-induced AC firing (Pre/Post Pairing); (iii) pairing of HFLS of EC→AC CCK^+ projection with SPLS of the VC→AC projection; (iv) HFLS of EC→AC CCK^+ projection followed by Pre/Post Pairing; (v) HFLS of VC→AC projection followed by Pre/Post Pairing; (vi) testing different parameters of the pairing protocol: the frequency of the laser stimulation of the EC→AC CCK^+ projection; the delay between the termination of HFLS of EC→AC CCK^+ projection and Pre/Post Pairing (Delay 1); and the delay between presynaptic activation of VC→AC projection and postsynaptic auditory cortex activation (Delay 2). Of particular interest was testing spike timing-dependent plasticity (STDP), an extension of the Hebbian learning rule, stating: in order to induce potentiation, the critical window between arrival of presynaptic input and postsynaptic firing should not be more than 20 ms (Bi and Poo, 1998; Markram et al., 1997; Zhang et al., 1998). This theory has been

challenged(Bittner et al., 2017; Drew and Abbott, 2006; Izhikevich, 2007), and we hypothesized that endogenous CCK could be involved in a type of synaptic potentiation that is different from STDP. Secondly, in behavioral experiments we examined, if infusion of a CCK *antagonist* in the AC could block the visuo-auditory association, and if a CCK *agonist* could rescue the deficit of visuo-auditory association in $CCK^{-/-}$ mice. Our results further support an important role of CCK for associative memory under natural conditions. Finally, we combined retrograde tracing and RNAscope in situ hybridization to explore CCK expression levels in the EC neurons projecting to the AC versus the projection from the VC.

Results

The auditory cortex receives a direct projection from the visual cortex

To examine the origin of the visual information underlying the previously observed visual responses in the AC(Chen et al., 2013; Li et al., 2014), we injected the retrograde tracer cholera toxin subunit B (Alexa Fluor 488 Conjugate, Molecular Probes, US) in the AC. The auditory thalamus was strongly labeled in the dorsal (MGD), ventral (MGV), and medial (MGM) subdivisions (Figure 1A1, 2). Many retrogradely labeled neurons were observed in both the primary and associative VC (Figure 1A3, 4), and were mostly distributed in layer V (Figure 1A4). The result here is consistent with previous studies reporting the existence of reciprocal projections between the VC and AC (Bizley et al., 2007; Budinger et al., 2006; Falchier et al., 2002; Falchier et al., 2010; Rockland and Ojima, 2003), and provides a possible anatomical basis for visuo-auditory associations formed in the AC.

High-frequency stimulation of VC→AC projection does not induce LTP

High-frequency stimulation (HFS) is a classical protocol to induce LTP (Bashir et al., 1991; Bliss and Gardner-Medwin, 1973; Bliss and Lomo, 1973; Hernandez et al., 2005; Yun et al., 2002), which typically consists of 1 s train of pulses at 100 Hz repeated 3 times with an inter-trail interval (ITI) of 10 s. Based on the current understanding we should be able to induce LTP, if the VC→AC projection is activated with HFLS. We injected AAV9-syn-ChrimsonR-tdtomato in the VC of wildtype mice and manipulated the VC projection terminals in the AC expressing ChimsonR (Figures 1B), a variant of channelrhodopsin-2. Laser stimulation of the VC→AC projection (VALS) induced a field excitatory post-synaptic potential ($fEPSP_{VALS}$) in the AC as an indicator of the VC→AC input. To prevent photoelectric artifacts, fEPSPs evoked by laser stimulation were recorded by glass pipette electrodes with an impedance of 1 MΩ rather than

metal electrodes(Cardin et al., 2010; Kozai and Vazquez, 2015) (Figures S1A and S1B). Generally, a laser with higher intensity induced a fEPSP with a steeper slope and larger amplitude until saturation was reached (Figure 1C). Considering the kinetics of ChrimsonR (Klapoetke et al., 2014), we modified the HFS protocol and used 4 trials of 1 s pulse train at 80 Hz with an ITI of 10 s (Figure 1D upper). We chose the laser intensity that induced a 50% fEPSP saturation for baseline and the post-HFLS tests and 75% for HFLS. However, no significant LTP was induced in the VC→AC projection by HFLS of this pathway alone (Figure 1D bottom, $p = 0.403$, $n = 10$, paired t-test).

VC→AC inputs are potentiated after pairing the activation of their terminals with noise bursts in the presence of CCK

Hebbian theory says that cells that fire together wire together. We next tested if VC→AC inputs can be potentiated after pairing with repetitive AC activation. We used VALS to evoke presynaptic input and noise stimulus to trigger postsynaptic AC firing. Since the latency of $fEPSP_{VALS}$ is approximately 2–2.5 ms, and the firing latency of noise responses in the AC of mice is mostly equal to or longer than 13 ms, we presented the laser stimulus 10 ms after noise. Therefore, we started the presynaptic input just before the postsynaptic firing (Pre/Post Pairing, Figure 1E). Responses to noise at different sound intensities were first tested (Figure 1F), and we chose the intensity that evoked reliable firing for Pre/Post Pairing. However, even after 80 trials of Pre/Post Pairing, the VC→AC inputs were not potentiated (Figure 1G, gray, ACSF group).

In the previous studies we have shown that CCK has an important role in neocortical plasticity (Chen et al., 2019; Li et al., 2014; Zhang et al., 2020). We then examined if VC→AC inputs could be potentiated after Pre/Post Pairing in the presence of CCK. Before Pre/Post Pairing, CCK-8S (10 ng/μL, 0.5 μL, 0.1 μL/min; Tocris Bioscience, Bristol, UK) was infused in the AC. In line with our hypothesis, VC→AC inputs were strongly potentiated after infusion of CCK-8S compared with ACSF. The averaged $fEPSP_{VALS}$ slope increased immediately after pairing and remained elevated for 1 h in the CCK injection group (Figures 1G and S1C, two-way repeated measures [RM] ANOVA, $F_{(1,27)} = 25.125$, significant interaction, $p < 0.001$; red, CCK before [101.3±0.8%] vs. CCK after [136.5±7.7%], pairwise comparison, $p < 0.001$, $n = 14$; gray, ACSF before [99.9±0.8%] vs. ACSF after [95.3±2.9%], pairwise comparison, $p = 0.411$, $n = 15$). Collectively, these results provide evidence that CCK together with noise, but not noise alone, enables a visuo-auditory association in the AC via a direct projection from the VC to AC.

178

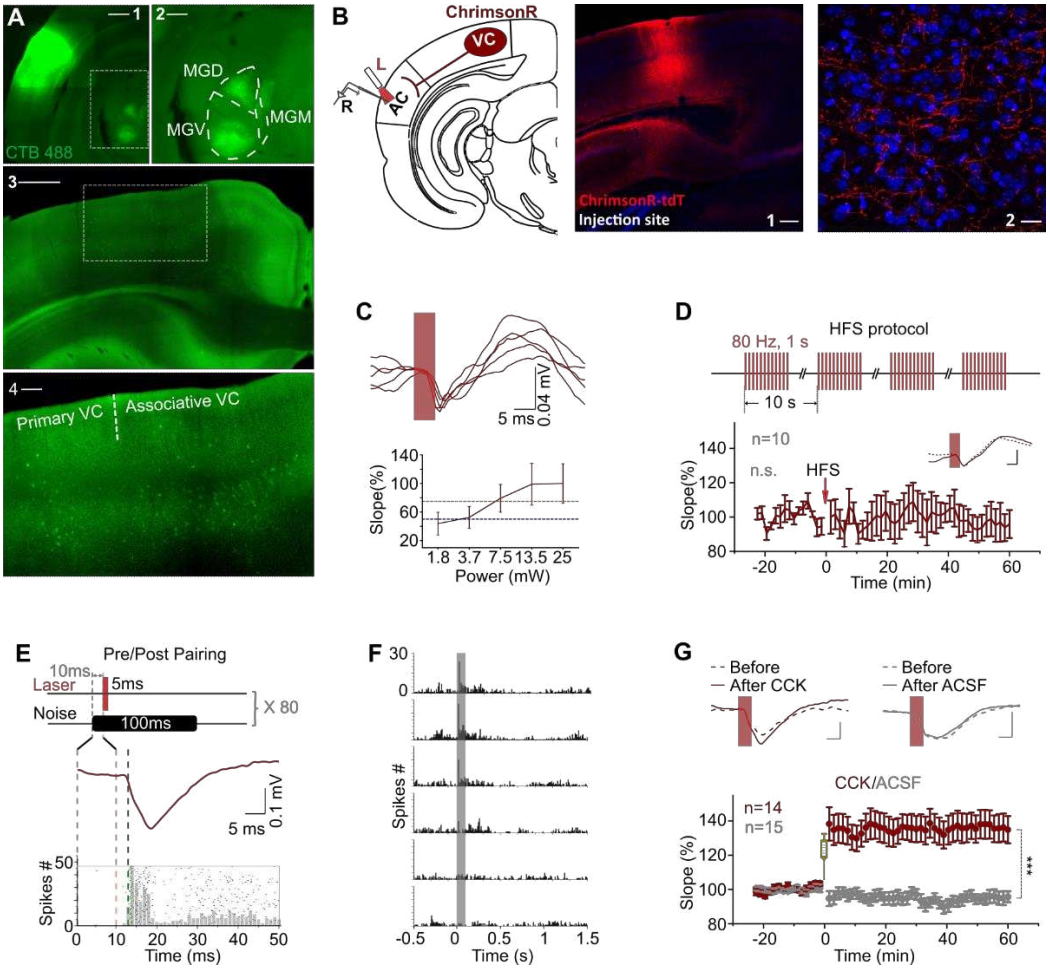

Figure 1. VC→AC projection was potentiated after pairing VALS evoked presynaptic activation with noise induced postsynaptic firing in the presence of CCK.

(A) Images show the injection site of the retrograde tracer (CTB488) in the AC (A_1, scale bar: 1000 µm) and retrogradely labeled neurons in the auditory thalamus (A_2, an enlargement of the boxed area in the A_1, scale bar: 500 µm) and the VC (A_3, scale bar: 1000 µm; A_4, an enlargement of the boxed area in A_3, scale bar: 200 µm). MGV, MGD, and MGM are abbreviations for the ventral, dorsal, and medial parts of the medial geniculate nucleus, respectively.

(B) Left: schematic drawing of the experimental setup. AAV9-syn-ChrimsonR-tdtomato was injected in the VC. L, laser fiber; R, recording electrode. Right: representative images of the injection site in the VC (1) and the projection terminals in the AC (2). Scale bars: 1, 200 µm; 2, 20 µm.

(C) Example fEPSP traces evoked by laser stimulation at different intensities (upper) and the corresponding input/output curve (bottom). Blue and yellow dashed line indicate 50% and 75% of fEPSP saturation.

(D) Upper: modified HFS protocol. Bottom: normalized $fEPSP_{VALS}$ slopes before and after HFLS of VC→AC projection alone; inset, example traces before (dashed) and after (solid) HFLS. Error bars represent SEM. paired t-test, $t(9) = 0.878$, n.s. $p = 0.403$, $n = 10$.

(E) The protocol of pairing VALS evoked presynaptic input with noise induced postsynaptic firing.

(F) PSTHs of spike responses to noises at different sound intensities (40 to 90 dB, from bottom to top).

(G) Normalized $fEPSP_{VALS}$ slopes (bottom) and example traces (upper) before and after Pre/Post Pairing with CCK-8S (red) or ACSF (gray) infusion in the AC. Error bars represent SEM. *** $p < 0.001$, $n = 14$ for CCK group, $n = 15$ for ACSF group, two-way RM ANOVA with Bonferroni post-hoc test.

See Table S1 for detailed Statistics.

179

180

HFLS of EC→AC CCK⁺ terminals results in LTP of VC→AC inputs after pairing with postsynaptic firing in the AC evoked by noise stimuli

We have shown that cortical projection neurons in the EC mostly are CCK$^+$ and glutamatergic, and that HFS induces CCK release in the auditory cortex (Chen et al., 2019). We then explored if endogenous CCK could enable the potentiation of VC→AC inputs. With Chronos and ChrimsonR (Klapoetke et al., 2014), we were able to manipulate two different neural pathways with two color activation. We injected AAV9-Ef1α-Flex-Chronos-GFP and AAV9-hSyn-ChrimsonR-tdTomato in the EC and VC of the CCK-iRES-Cre mouse to activate the EC→AC CCK$^+$ projection and VC→AC projection, respectively (Figure 2A). HFLS (473 nm 80 Hz, 5-ms/pulse, 10 pulses, Figure S2C left) of the EC→AC CCK$^+$ projection was applied and, after a 10-ms interval, pairing of VALS (635 nm) and noise stimulus was followed (Figure 2C, HFLSEA/Pre/PostPairing). This protocol was repeated for 5 trials with an ITI of 10s. Likewise, we injected AAV9-Ef1α-Flex-Chronos-GFP in the VC of CaMKIIa-Cre mice (Figure 2B) and applied 5 trials of HFLS of VC→AC projection (Figure S2C right) followed by the pairing of VALS and noise stimulus (Figure 2D, HFLSVA/Pre/PostPairing).

The VC→AC inputs were potentiated when we applied HFLS on the EC→AC CCK$^+$ projection but not on the VC→AC projection (Figures 2E, LTP curves; 2F, fEPSP traces; 2G, two-way RM ANOVA, $F_{(1,21)} = 10.490$, significant interaction, $p = 0.004$; red, HFLSEA/Pre/PostPairing before [99.9±1.5%] vs. after [120.7±4.0%], pairwise comparison, $p < 0.001$, $n = 13$; green, HFLSVA/Pre/PostPairing before [99.9±2.0%] vs. after [97.2±6.7%], pairwise comparison, $p = 0.623$, $n = 10$; HFLSEA/Pre/PostPairing after vs. HFLSVA/Pre/PostPairing after, pairwise comparison, $p = 0.005$). However, simple pairing of HFLS of EC→AC, CCK$^+$ projection with single pulse VALS did not potentiate the VC→AC input (Figure S2D, $t_{(8)} = -0.899$, $p = 0.395$, $n = 9$, paired t-test). This may be interpreted as lack of Hebbian postsynaptic activation and agree with our previous study (Li et al., 2014). Besides, fEPSPs evoked by noise stimuli (acoustic stimuli, AS) were also potentiated after HFLSEA/Pre/PostPairing but not HFLSVA/Pre/PostPairing (Figures 2H, LTP curves; 2I, fEPSP traces; 2J, two-way RM ANOVA, $F_{(1,16)} = 9.711$, significant interaction, $p = 0.007$; black, HFLSEA/Pre/PostPairing before [100.4±1.2%] vs. after [143.2±14.9%], pairwise comparison, $p = 0.001$, $n = 8$; gray, HFLSVA/Pre/PostPairing before [101.7±0.5%] vs. after [100.5±2.3%], pairwise comparison, $p = 0.898$, $n = 10$; HFLSEA/Pre/PostPairing after vs.

HFLSVA/Pre/PostPairing after, pairwise comparison, $p = 0.006$). However, the EC→AC, CCK^+ inputs were not significantly potentiated after HFLSEA/Pre/PostPairing (Figures 2K, LTP curves; 2L, fEPSP traces; 2M, paired t-test, $t_{(12)} = -1.424$, $p = 0.180$, $n = 13$). The results suggest that HFLS of EC→AC CCK^+ projection rather than VC→AC $CaMKII^+$ projection is necessary to induce potentiation of VC→AC inputs, whereby CCK release induced by the former one is an underpinning mechanism. Taken together, our results demonstrate a typical form of heterosynaptic plasticity, in which the potentiation of the VC→AC input is not dependent on HFLS of its own pathway but requires HFLS of the EC→AC projection that presumably triggers CCK release.

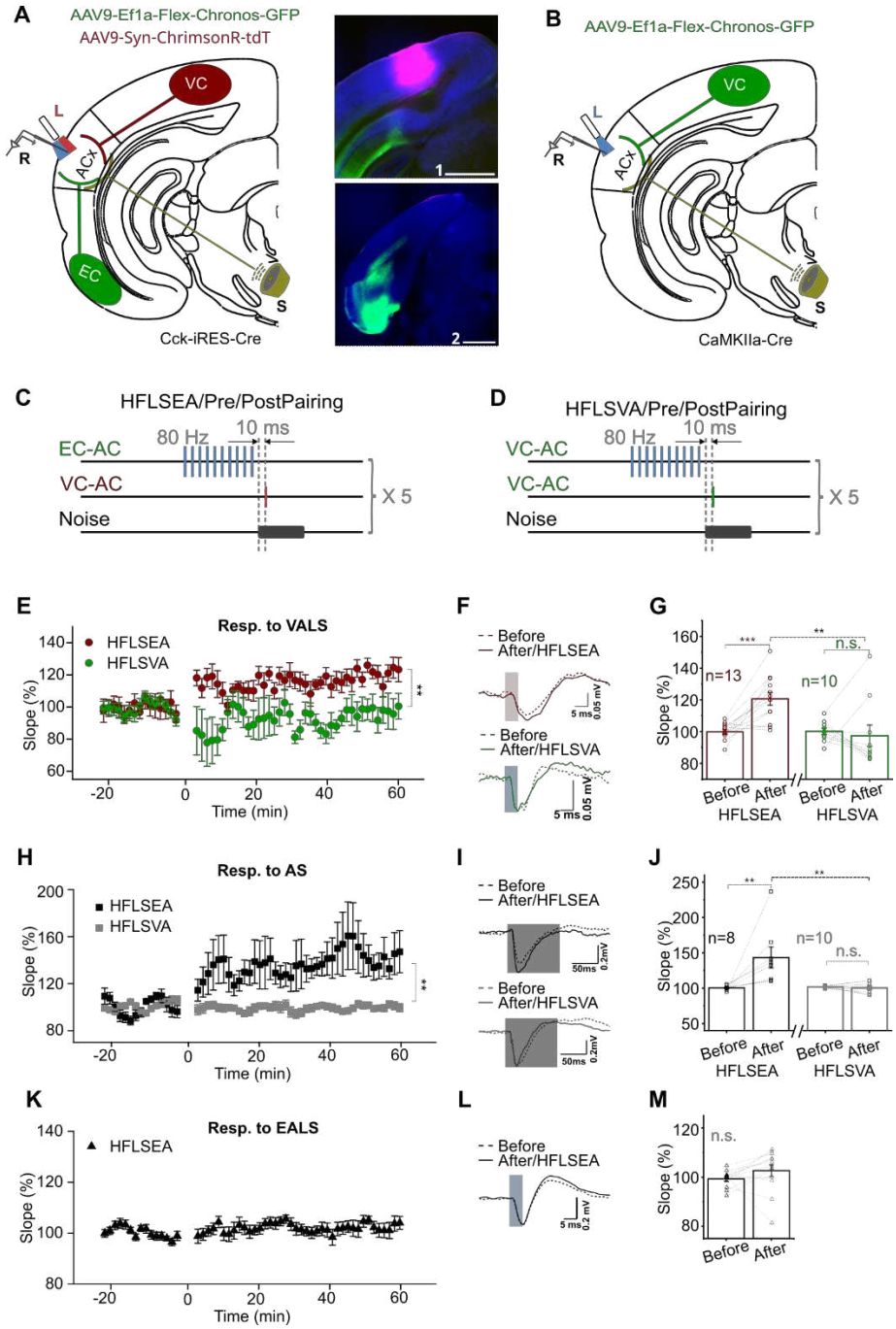

Figure 2. HFLS of EC→AC CCK$^+$ projection but not VC→AC projection induced the potentiation of VC→AC inputs after pairing with noise evoked postsynaptic activation.
(A) Left: schematic drawing of the experimental setup. AAV9-Ef1α-Flex-Chronos-GFP and AAV9-Syn-ChrimsonR-tdTomato were injected in the EC and VC of CCK-iRES-Cre mice respectively. Right: representative images of the injection sites in the VC (1) and the EC (2). Scale bars: 1, 1000 μm; 2, 1000 μm. L, laser fiber; R, recording electrode; S, sound.
(B) Schematic drawing of the experimental setup. AAV9-Ef1α-Flex-Chronos-GFP was injected in the VC of CaMKIIa-cre mice. L, laser fiber; R, recording electrode; S, sound.
(C) and (D) Protocols of HFLSEA/Pre/PostPairing and HFLSVA/Pre/PostPairing, respectively.
(E) Normalized fEPSP$_{VALS}$ slopes before and after HFLSEA/Pre/PostPairing (red) or HFLSVA/Pre/PostPairing (green). ** $p < 0.01$, two-way RM ANOVA with post-hoc Bonferroni test.
(F) Example fEPSP$_{VALS}$ traces before and after HFLSEA/Pre/PostPairing (red) or HFLSVA/Pre/PostPairing (green). Scale bars: upper, 5 ms and 0.05 mV; bottom, 5 ms and 0.05 mV.
(G) Individual and average fEPSP$_{VALS}$ slope changes before and after HFLSEA/Pre/PostPairing (red) or HFLSVA/Pre/PostPairing (green). ** $p < 0.01$, *** $p < 0.001$, n.s. $p = 0.623$, $n = 13$ for HFLSEA/Pre/PostPairing group, $n = 10$ for HFLSVA/Pre/PostPairing group, two-way RM ANOVA with post-hoc Bonferroni test.
(H) Normalized fEPSP$_{AS}$ slopes before and after HFLSEA/Pre/PostPairing (black) or HFLSVA/Pre/PostPairing (gray). ** $p < 0.01$, two-way RM ANOVA with post-hoc Bonferroni test.
(I) Example fEPSP$_{AS}$ traces before and after HFLSEA/Pre/PostPairing (black) or HFLSVA/Pre/PostPairing (gray). Scale bars: upper, 50 ms and 0.2 mV; bottom, 50 ms and 0.2 mV.
(J) Individual and average fEPSP$_{AS}$ slope changes before and after HFLSEA/Pre/PostPairing (black) or HFLSVA/Pre/PostPairing (gray). ** $p < 0.01$, n.s. $p = 0.898$, $n = 8$ for HFLSEA/Pre/PostPairing group, $n = 10$ for HFLSVA/Pre/PostPairing group, two-way RM ANOVA with post-hoc Bonferroni test.
(K) Normalized fEPSP$_{EALS}$ slopes before and after HFLSEA/Pre/PostPairing.
(L) Example fEPSP$_{EALS}$ traces before and after HFLSEA/Pre/PostPairing. Scale bars: upper, 5 ms and 0.2 mV.
(M) Individual and average fEPSP$_{EALS}$ slope changes before and after HFLSEA/Pre/PostPairing. paired t-test, $t_{(12)} = -1.424$, n.s. $p = 0.180$, $n = 13$.
See Table S1 for detailed Statistics.

HFLS of EC→AC CCK⁺ terminals in vitro leads to LTP of VC→AC inputs after pairing with electrical stimulation

We also performed similar experiments at the single cell level in vitro. Slices were prepared from CCK-iRES-Cre mice after injection of AAV9-Ef1α-Flex-Chronos-GFP in the EC and of AAV9-Syn-ChrimsonR-tdTomato in the VC (Figure 3A). Pyramidal neurons in the auditory cortex were patched (Figure 3B), and excitatory postsynaptic currents evoked by VALS ($EPSC_{VALS}$, Figure 3C) and electrical stimulation of the auditory cortex ($EPSC_{ESAC}$, Figure 3D) were recorded. HFLS of the EC→AC CCK^+ projection (Figure 3E) was followed by the pairing of VALS and postsynaptic activation evoked by ESAC, which was repeated for 5 times with an ITI of 10s (Figure 3F left). As a control, we replaced the HFLS of EC→AC CCK^+ projections with HFLS of VC→AC projection (Figure 3F right).

Similar to the *in vivo* results, the amplitude of $EPSC_{VALS}$ significantly increased after HFLSEA/Pre/PostPairing but not after HFLSVA/Pre/PostPairing (Figures 3G, LTP curves; 3H, $EPSC_{VALS}$ traces; 3I, two-way RM ANOVA, $F_{(1,12)}$= 5.759, significant interaction, p = 0.034; red, increased by 22.2 ± 10.1% after HFLSEA/Pre/PostPairing, pairwise comparison, p = 0.012, n = 7; gray, changed by 3.3 ± 3.2% after HFLSVA/Pre/PostPairing, pairwise comparison, p = 0.670, n = 7; HFLSEA/Pre/PostPairing after [122.2 ± 10.1%] vs. HFLSVA/Pre/PostPairing after [96.7 ± 3.2%], pairwise comparison, p = 0.034; S3A and S3B, 10 successive example traces and their averaged trace of the EPSCs at different time points as shown in Figure 3G). Likewise, the $EPSC_{ESAC}$ amplitude increased by 42.4 ± 7.9% after HFLSEA/Pre/PostPairing but not after HFLSVA/Pre/PostPairing (Figures 3J, LTP curves; 3K, $EPSC_{ESAC}$ traces; 3L, two-way RM ANOVA, $F_{(1,12)}$=28.074, significant interaction, p < 0.001; black, HFLSEA/Pre/PostPairing before vs. after, pairwise comparison, p < 0.001, n = 7; gray, changed by 1.4 ± 5.8% after HFLSVA/Pre/PostPairing, pairwise comparison, p = 0.814, n = 7; HFLSEA/Pre/PostPairing after [142.4 ± 7.9%] vs. HFLSVA/Pre/PostPairing after [98.6 ± 2.5%], pairwise comparison, p < 0.001; S3C and S3D, 10 successive traces and their averaged trace at different timepoints as shown in Figure 3J). These results, from recording at the synaptic level, provide further evidence for the view that HFLS of EC→AC, CCK^+ projection is a prerequisite to potentiate the VC inputs to the AC.

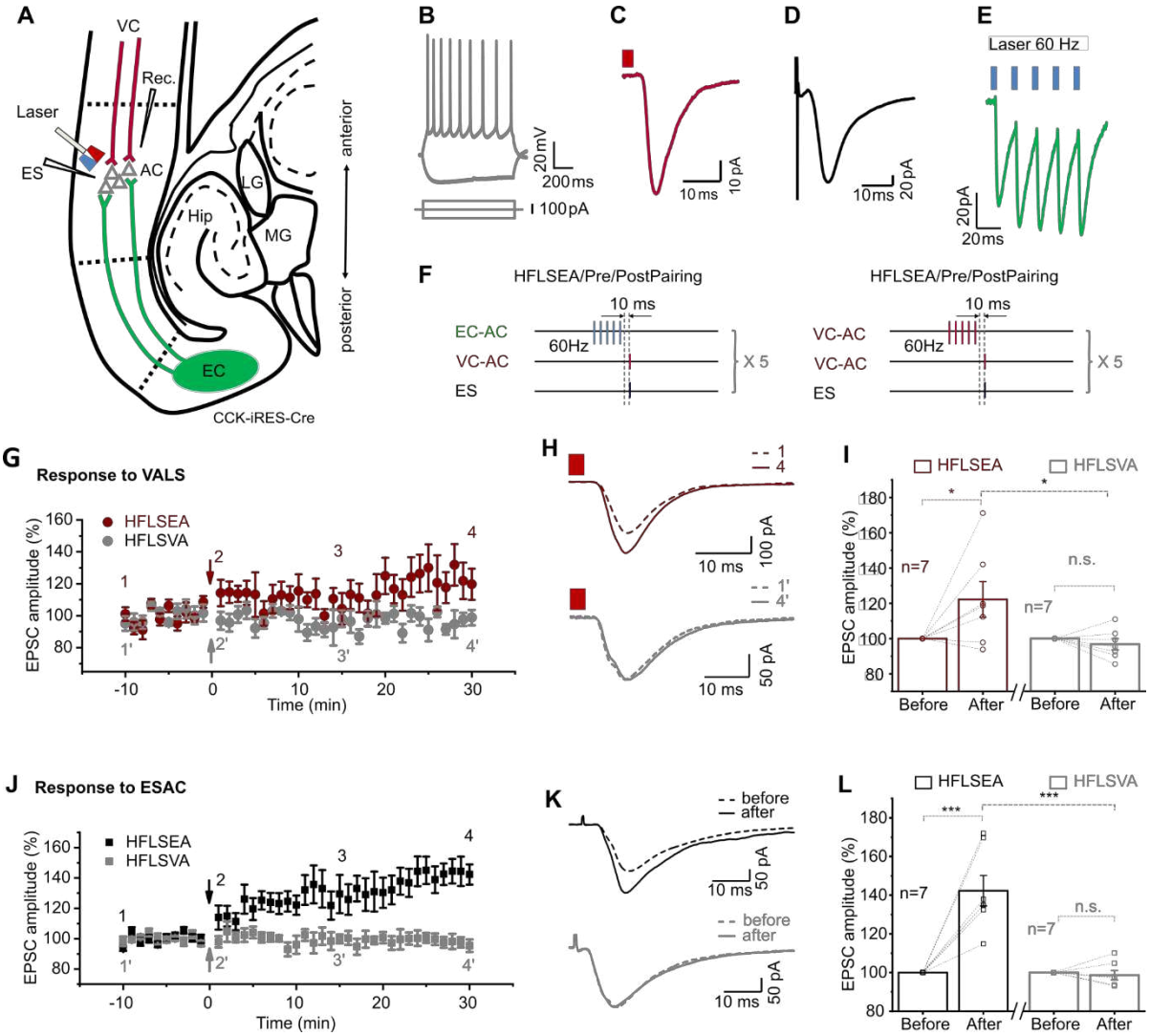

Figure 3. HFLS of ENT→AC CCK⁺ terminals in vitro leads to LTP of VC→AC inputs after pairing with electrical stimulation

(A) Positions of the whole cell recording pipette, electrical stimulation electrode, and the optical fiber in a slice of CCK-iRES-Cre mice with AAV-Ef1α-Flex-Chronos-GFP injected in Ent and AAV-Syn-ChrimsonR-tdTomato injected in VC.

(B) Representative pyramidal neuron firing in response to current injection.

(C and D) Representative traces of $EPSC_{VALS}$ (C) and $EPSC_{ESAC}$ (D) of pyramidal neuron. Scale bars: C, 10 ms and 10 pA; D, 10 ms and 20 pA.

(E) Representative EPSC trace in response to HFLS of Ent→AC CCK⁺ terminals (blue rectangles, 60 Hz, 3 ms/pulse, 5 pulses).

(F) Protocols of HFLSEA/Pre/PostPairing (left) and HFLSVA/Pre/PostPairing (right).

(G) Normalized $EPSC_{VALS}$ amplitudes before and after HFLSEA/Pre/PostPairing (red) or HFLSVA/Pre/PostPairing (gray).

(H) Example $EPSC_{VALS}$ traces before (dashed, at timepoint 1 or 1' in G) and after (solid, at timepoint 4 or 4' in G) HFLSEA/Pre/PostPairing (red, upper) or HFLSVA/Pre/PostPairing (gray, bottom).

(I) Individual and average $EPSC_{VALS}$ amplitude changes before and after HFLSEA/Pre/PostPairing (red) or HFLSVA/Pre/PostPairing (gray). * $p < 0.05$, n.s. $p = 0.670$, n = 7 for HFLSEA/Pre/PostPairing group, n = 7 for HFLSVA/Pre/PostPairing group, two-way RM ANOVA with post-hoc Bonferroni test.

(J) Normalized $EPSC_{ESAC}$ amplitudes before and after HFLSEA/Pre/PostPairing (black) or HFLSVA/Pre/PostPairing (gray).

(K) Example $EPSC_{ESAC}$ traces before (dashed, at timepoint 1 or 1' in J) and after (solid, at timepoint 4 or 4' in J) HFLSEA/Pre/PostPairing (black, upper) or HFLSVA/Pre/PostPairing (gray, bottom).

(L) Individual and average $EPSC_{ESAC}$ amplitude changes before and after HFLSEA/Pre/PostPairing (red) or HFLSVA/Pre/PostPairing (gray). *** $p < 0.01$, n.s. $p = 0.814$, n = 7 for HFLSEA/Pre/PostPairing group, n = 7 for HFLSVA/Pre/PostPairing group, two-way RM ANOVA with post-hoc Bonferroni test.

See Table S1 for detailed Statistics.

254

EC→AC projecting neurons have higher CCK expression levels than VC→AC projecting neurons

A variety of neuropeptides, including CCK, are expressed in the neocortex, mostly in interneurons (Somogyi and Klausberger, 2005), although CCK is also expressed in projection neurons. The results in the present study indicate that HFLS of the EC→AC, but not of the VC→AC, projection can produce LTP in AC. We next explored if levels of CCK transcript, and thus possibly CCK peptide, could underly this difference by using RNAscope combined with retrograde tracing with AAV virus. We injected AAVretro-hSyn-Cre-WPRE-hGH in the AC of Ai14 mice, a Cre reporter line, retrogradely labeling the EC and VC neurons projecting to AC with Cre-dependent tdTomato. The expression level of CCK was then assessed by RNAscope, a semi-quantitative *in situ* hybridization method (Figure 4A-D). We found that the *expression level* of CCK was significantly higher among projecting neurons in the EC than in the VC across three animals analyzed (Figures 4E and S4). The *proportion* of projecting neurons expressing elevated CCK levels was also higher in the EC compared with the VC (Figure 4F). These results suggest that after HFLS more CCK is released from EC→AC neurons than from VC→AC neurons, which may, at least, be one explanation why the former but not the latter can produce LTP.

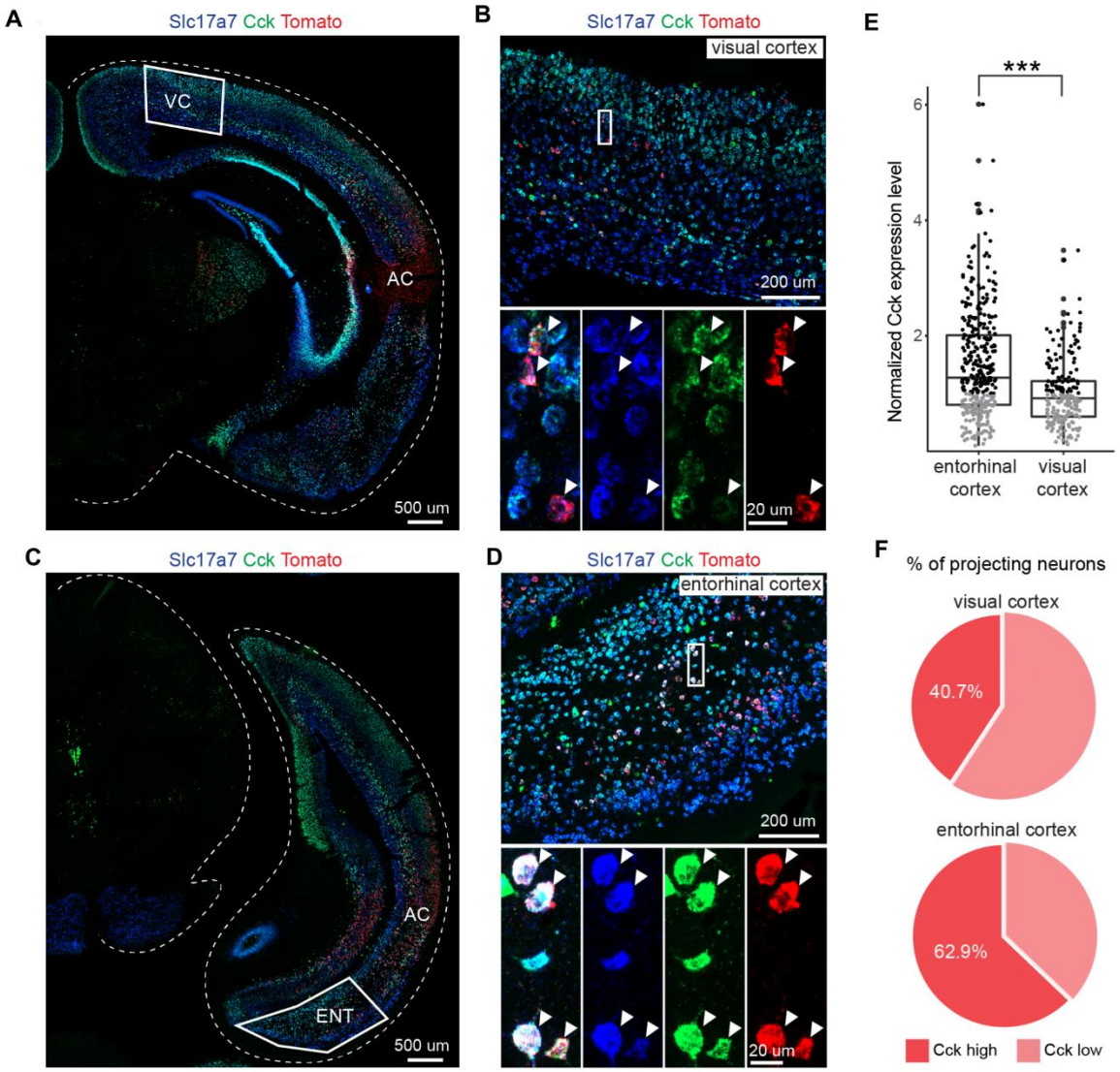

Figure 4. AC projection neurons in the Ent express higher level of CCK than that in the VC.
(A) Overview of injection site at the AC and projecting neurons in the VC. Scale bar: 500 um.
(B) Expression of Slc17a7 (vGlut1) and Cck in retrogradely labeled neurons (tdTomato+) in the VC. Scale bars: upper, 200 µm; bottom, 20 µm.
(C) Overview of injection site at the AC and projecting neurons in the Ent. Scale bar: 500 µm. (D) Expression of Slc17a7 and Cck in retrogradely labeled neurons (tdTomato+) in the EC. Scale bars: upper, 200 µm; bottom, 20 µm.
(E) Comparison of Cck expression level in AC projecting neurons of EC and VC (data points are from 3 animals). unpaired t-test, ***p<0.001. Black, high level; gray, low level.
(F) Pie chart showing percentage of projecting neurons expressing low and high Cck level in the VC (upper) and the EC (bottom), respectively.
See Table S1 for detailed Statistics.

271

Effect of different parameters of the pairing protocol on the potentiation level of VC→AC inputs

Neuropeptide release likely is frequency-dependent (Bean and Roth, 1991; Hökfelt, 1991; Iverfeldt et al., 1989; Lundberg and Hokfelt, 1983; Shakiryanova et al., 2005; Whim and Lloyd, 1989), and our results suggest that CCK released from the EC→AC CCK^+ projection was critical for generating visuo-auditory cortical LTP. We hypothesized that the frequency of the laser used to stimulate the EC→AC CCK^+ projection was critical for the level of potentiation of the VC→AC input. We therefore varied the *frequency of the laser stimulation* (80, 40, 10, or 1 Hz). As shown in Figure 5A left, the delay between the termination of repetitive laser stimulation of the CCK^+ EC→AC projection and presynaptic activation (Delay 1) was set at 10 ms, and the delay between pre and postsynaptic activation (Delay 2) was set at 0 ms. The potentiation level of the VC→AC inputs showed a tendency to increase as the frequency of laser stimulation of the CCK^+ EC→AC projection increased (Figure 5A right, two-way RM ANOVA, $F_{(3,34)} = 10.666$, significant interaction, $p < 0.001$; 1 Hz before [99.7 ± 1.3%] vs. after [96.6 ± 2.9%] , pairwise comparison, $p = 0.352$, n =9; 10 Hz before [98.5 ± 1.2%] vs. after [105.8 ± 2.5%] , pairwise comparison, p =0.044, n = 8; 40 Hz before [99.4 ± 0.8%] vs. after [110.5 ± 1.8%] , pairwise comparison, $p = 0.003$, n=8; 80 Hz before [99.9 ± 1.5%] vs. after [120.7 ± 4.0%] , pairwise comparison, $p < 0.001$, n = 13). If higher than 10 Hz, the VC→AC input was significantly potentiated. However, at 1 Hz no significant potentiation was observed.

In contrast to small-molecule neurotransmitters that are rapidly cleared by reuptake pumps, neuropeptides are mostly released extra-synaptically, are removed/inactivated more slowly, and may have longer-lasting effects. Thus, we explored the role of Delay 1, i.e. if the *time* interval between the termination of HFLS and the Pre/Post Pairing influenced the degree of potentiation of the VC→AC inputs (Delay 2 = 0 ms, HFLS frequency = 80 Hz, Figure 5B left). The VC→AC inputs were significantly potentiated, when Delay 1 was 10, 85, 235, or 535 ms rather than 885 or -65 ms (Figure 5B right, two-way RM ANOVA, $F_{(5,59)} = 7.115$, significant interaction, $p < 0.001$; 10 ms before [99.9 ± 1.5%] vs. after [120.7 ± 4.0%]], pairwise comparison, $p < 0.001$, n = 13; 85 ms before [99.8 ± 0.8%] vs. after [119.1 ± 3.5%], pairwise comparison, $p < 0.001$, n= 13; 235 ms before [99.5 ± 3.7%] vs. after [117.0 ± 5.2%], pairwise comparison, $p < 0.001$, n= 6; 535 ms before [99.4 ± 0.6%] vs. after [110.4 ± 1.9%], pairwise comparison, $p = 0.003$, n= 10; 885 ms before [99.6 ± 0.8%] vs. after [102.7 ± 1.3%], pairwise

303 comparison, p = 0.385, n= 10; -65 ms before [99.0 ± 0.8%] vs. after [100.1 ± 3.0%], pairwise
304 comparison, p = 0.945, n= 13).

305 The Hebbian theory states, popularly, that "cells that fire together wire together"(Löwel
306 and Singer, 1992), a more accurate interpretation being 'synaptic strength increases when the
307 presynaptic neuron always fires immediately before the post-synaptic neuron'(Caporale and Dan,
308 2008). Based on this, the interval between pre and postsynaptic activation should be critical for
309 potentiation. In the next experiment, the interval (Delay 2) between VC→AC projection
310 activation (i.e., presynaptic activation) and natural auditory cortex activation (i.e., postsynaptic
311 activation) was set as the only variable (Delay 1 = 10 ms, HFLS frequency = 80 Hz, Figure 5C
312 left). The potentiation of VC→AC inputs showed a trend towards decrease as Delay 2 increased.
313 Significant potentiation was observed when Delay 2 was 0, 50, 200, rather than 400, 800 ms and
314 ∞ (without noise) (Figure 5C right, two-way RM ANOVA, F(5,51) =4.133, significant
315 interaction, p = 0.003; 0 ms before [99.9 ± 1.5%] vs. after [120.7 ± 4.0%]], pairwise comparison,
316 p < 0.001, n = 13; 50 ms before [99.7 ± 0.6%] vs. after [110.7 ± 2.7%], pairwise comparison, p =
317 0.001, n= 11; 200 ms before [102.0 ± 1.2%] vs. after [110.6 ± 3.3%], pairwise comparison, p =
318 0.006, n= 12; 400 ms before [97.5 ± 1.5%] vs. after [105.3 ± 2.1%], pairwise comparison, p =
319 0.073, n= 6; 800 ms before [98.6 ± 1.8%] vs. after [101.8 ± 2.1%], pairwise comparison, p =
320 0.454, n= 6; ∞ before [100.0 ± 1.3%] vs. after [103.2 ± 3.3%], pairwise comparison, p = 0.363,
321 n= 9).

322 Taken together, to induce a significant potentiation of VC→AC inputs (Figure 5D, black
323 cube) within five trails pairing with an ITI of 10 s, (i) the frequency of repetitive laser
324 stimulation of the CCK^+ EC→AC projection should be 10 Hz or higher, (ii) Delay 1 should be
325 longer than 10 ms and shorter than 535 ms, and (iii) Delay 2 should be longer than 0 ms and
326 shorter than 200 ms.
327
328
329

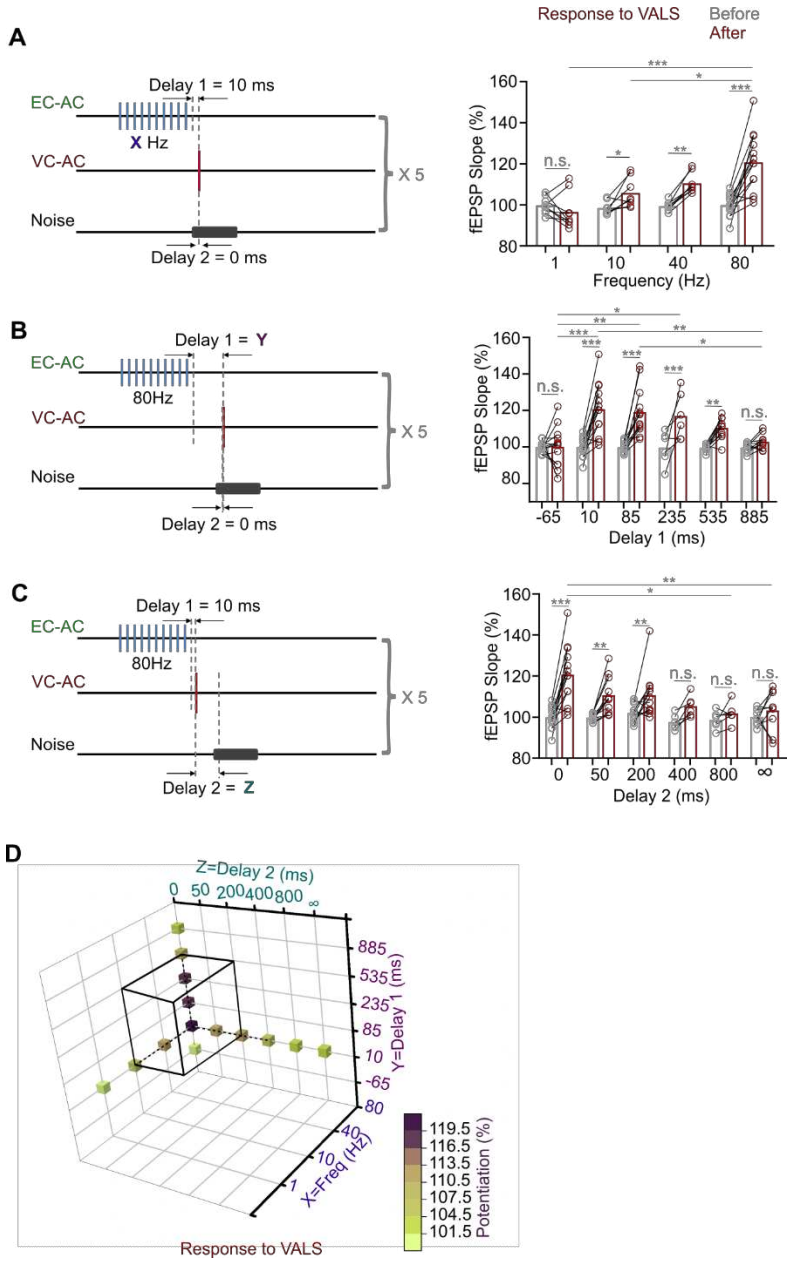

Figure 5. Effect of different parameters of the pairing protocol on the potentiation level of VC→AC inputs.

(A) Left: schematic drawing of experiment design. Delay1 =10 ms, Delay2 = 0 ms, and the frequency was varied (80, 40, 10, or 1 Hz). Right: individual and average $fEPSP_{VALS}$ slopes (normalized to the baseline) after pairing at different frequencies. Two-way RM ANOVA with post-hoc Bonferroni test, n.s. no significant, * $p < 0.05$, ** $p < 0.01$, *** $p < 0.001$, n = 9 for 1 Hz, n = 8 for 10 Hz, n = 8 for 40 Hz, n = 13 for 80 Hz. Data points in groups 1 Hz and 40 Hz refer to our previous study (Zhang et al., 2020).

(B) Left: schematic drawing of experiment design. HFLS Frequency = 80 Hz, Delay2 = 0 ms, and Delay 1 was varied (10, 85 235, 535, 885, and -65 ms). Right: individual and average $fEPSP_{VALS}$ slopes (normalized to the baseline) after pairing at different Delay1s. Two-way RM ANOVA with post-hoc Bonferroni test, n.s. no significant, * $p < 0.05$, ** $p < 0.01$, *** $p < 0.001$, n=13, 13, 13, 6, 10, 10 for Delay 1=-65, 10, 85, 235, 535, and 885 ms, respectively.

(C) Left: schematic drawing of experiment design. HFLS Frequency = 80 Hz, Delay1 = 10 ms, and Delay 2 was varied (0, 50, 200, 400, 800 ms, and ∞). Right: individual and average $fEPSP_{VALS}$ slopes (normalized to the baseline) after pairing at different Delay2s. Two-way RM ANOVA with post-hoc Bonferroni test, n.s. not significant, * $p < 0.05$, ** $p < 0.01$, *** $p < 0.001$, n = 13, 11, 12, 6, 6, 9 for Delay 2= 0, 50, 200, 400, 800 ms and ∞, respectively.

(D) Three-dimensional summary of the effect of different parameters (Frequency, Delay1 and Delay2) on the potentiation level of VC→AC inputs**.** Parameters locate inside black cubes can induce significant potentiation.

See Table S1 for detailed Statistics.

Application of a CCKBR antagonist blocks generation of the visuo-auditory association

The above results showed that the generation of visuo-auditory associations needed inputs from the EC together with high-frequency stimulation, presumably triggering CCK release from their terminals. Next, we ask whether or not CCK is essential for generation of visuo-auditory associations, which can be reflected in a behavioural context.

To that end, we examined the role of CCK in the formation of visuo-auditory associative memory in a fear response test (Figure 6A). First, a CCKB receptor (CCKBR) antagonist (L-365,260) or ACSF was injected bilaterally into the AC, followed by a 25-trial pairing session of the visual stimulus (VS) with the AS. We repeated the above drug and pairing session 4 times per day and on 3 consecutive days. On day 4, baseline tests for the freezing response to the AS and VS were performed (3 trials) before the mouse was fear conditioned to the AS. After fear conditioning, freezing responses to the AS and VS were further examined on day 5 (Figure 6A). As expected, mice showed no freezing response to the AS before conditioning, but a high freezing rate to the AS after conditioning (Video S3, S4, S7, S8; Figure 6B, ACSF-AS-Baseline [7.4 ± 3.2%] vs. ACSF-AS-Post intervention [67.8 ± 4.0%], $p < 0.001$, n = 9; L-365,260-AS-Baseline [5.8 ± 1.6%] vs. L-365,260-AS-Post intervention [67.5 ± 4.1%], $p < 0.001$, n = 8; two-way RM ANOVA with post-hoc Bonferroni test). The ACSF mice group showed a significantly increased freezing response to the VS, indicating that an association between the AS and VS had been established during the pairings (Videos S1, S2; Figure 6B blue, ACSF-VS-Baseline [4.1 ± 0.9%] vs. ACSF-VS-Post intervention [24.4 ± 3.8%], $p<0.001$, n = 9, two-way RM ANOVA with post-hoc Bonferroni test). However, the bilateral infusion of L-365,260 into the AC blocked this association, resulting in a nil response to the VS (Video S5, S6; Figure 6B red, L-365,260-VS-Baseline [4.3 ± 1.2%] vs. L-365,260-VS-Post intervention [2.5 ± 1.6%], $p = 1.000$, n = 8, two-way RM ANOVA with post-hoc Bonferroni test). Mice showed a promising association between the AS and foot shock, as indicated by high freezing rate following the AS. However, an association between the VS and AS was not established. There was a significant difference between the freezing rates to the VS of experimental and control groups (Figure 6B; L-365,260-VS-Post intervention [2.5 ± 1.6%, n = 8] vs. ACSF-VS-Post intervention [24.4 ± 3.8%, n = 9], $p < 0.001$, two-way RM ANOVA with post-hoc Bonferroni test). These results demonstrate that the CCKBR antagonist prevented the generation of the association between the VS and AS and suggest an essential role of CCK in the generation of the visuo-auditory association.

Systemic administration of CCK4 rescues the deficit of CCK$^{-/-}$ mice in visuo-auditory memory

As seen after treatment with a CCK antagonist, we expected that CCK$^{-/-}$ mice would show a deficit in the formation of associative memory, and we tested this hypothesis (Figure 6C). Our previous results demonstrated that 6-9 trials were needed for CCK$^{-/-}$ mice to produce a freezing rate of >60% in response to the conditioned AS, whereas only 3 trials were needed for wild-type mice, suggesting a general associative learning deficit in the CCK$^{-/-}$ mice (Chen et al., 2019). The CCK$^{-/-}$ mice in the control group (with saline injection) consistently showed a minimal freezing response to VS after visuo-auditory association and fear conditioning (Videos S9-12; Figure 6D blue). To determine whether systemic administration of CCK could rescue this deficit, we administrated CCK-4 through a drug infusion cannula implanted into the transverse sinus. There is evidence that the tetrapeptide CCK-4 can penetrate the blood-brain barrier (Rehfeld, 2000). The CCK-4 dosage (1ug/kg) was at sub-panic attack level, and animals showed no sign of panic or anxiety after administration (Figure S5). CCK-4 injection resulted in a significantly higher freezing rate compared to the controls (Videos S13-16; Figure 6D red, CCK-VS-Post intervention [41.9 ± 5.6%, n = 7] vs. Saline-VS-Post intervention [10.0 ± 1.1%, n = 7], $p < 0.001$; two-way RM ANOVA with post-hoc Bonferroni test), indicating that the visuo-auditory association was rescued upon CCK4 administration.

To better compare the strength of visuo-auditory association under different experimental conditions, we calculated the ratio of the freezing response to the VS compared with that to the AS after conditioning (Figure 6E). The ratio of the CCKBR antagonist (L-365,260)-treated group was lowest among all groups, demonstrating a nearly complete abolishment of the visuo-auditory association. Interestingly, the ratio of the CCK-4 group was the highest among all groups (Figure 6E. $F_{(3, 27)} = 28.797$, CCK-4 infusion in CCK$^{-/-}$ mice [69.5 ± 6.2%, n = 7] vs. ACSF infusion in the wild-type mice [38.8 ± 7.3%, n = 9], $p = 0.002$, one-way ANOVA with post-hoc Bonferroni test). This result indicates a possible compensatory upregulation of CCK receptors in CCK$^{-/-}$ mice, leading to the highest association between the VS and AS, findings that are worth further investigation.

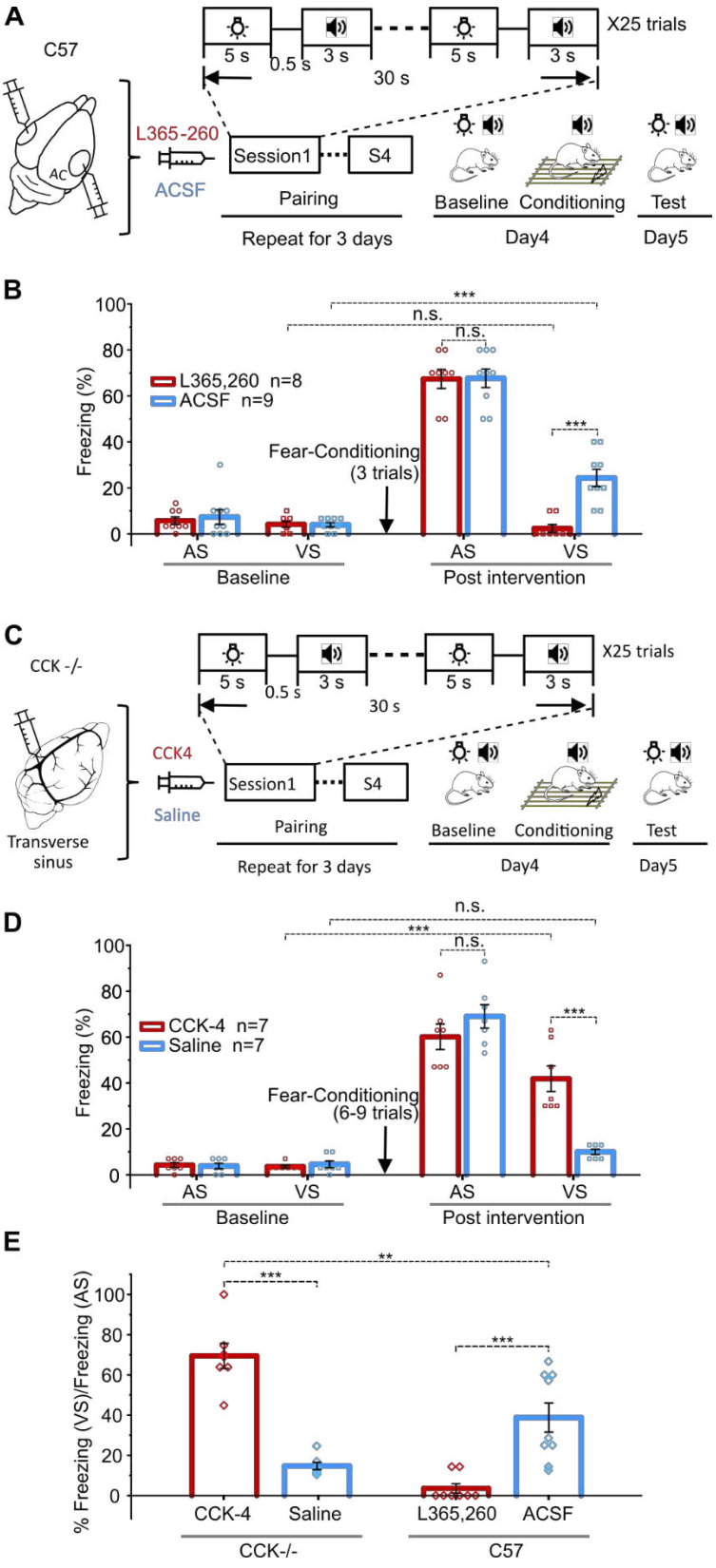

Figure 6. Visuo-auditory associative memory could not be formed without CCK.
(A) Schematic drawing of the training protocol for wild-type mice to associate the VS and AS. L-365,260 or ACSF was infused to the AC before pairing of VS and AS.
(B) Bar chart showing freezing percentages to the AS and VS before and after the conditioning. *** p<0.01, n.s. p = 1.000 for L-365,260-VS-Baseline vs. L-365,260-VS-Post intervention, n.s. p = 0.962 for L-365,260-AS-Post intervention vs. ACSF-AS-Post intervention, n=8 for L-365,260 group, and n = 9 for ACSF group, two-way RM ANOVA with post-hoc Bonferroni test.
(C) Schematic drawing of the training protocol for $CCK^{-/-}$ mice to associate the VS and AS. CCK-4 or ACSF was systemically administrated through the drug infusion cannula in the transverse sinus before paring of VS and AS.
(D) Bar chart showing freezing percentages of $CCK^{-/-}$ mice to the VS and AS before and after the intervention. *** p<0.01, n.s. p = 1.000 for Saline-VS-Baseline vs. Saline-VS-Post intervention, n.s. p = 0.264 for CCK-AS-Post intervention vs. Saline-AS-Post intervention, n=7 for CCK-4 group, and n = 7 for Saline group, two-way RM ANOVA with post-hoc Bonferroni test.
(E) The ratio of freezing in response to the VS over that to the AS after the intervention of wild-type and CCK-/- in all conditions are summarized in the bar chart. ** p<0.01, *** p<0.001, one-way ANOVA with post-hoc Bonferroni test.
See Table S1 for detailed Statistics.

Discussion

In the present study we demonstrate, in the mouse, that a direct input from the VC to the AC can be potentiated after pairing with postsynaptic firing evoked by auditory stimuli in the presence of CCK. This was observed both after exogenous administration and presumably after endogenous CCK release after HFLS of the CCK^+ EC→AC projection. In fact, a significant potentiation of the presynaptic input could be induced after only five trials of pairing, even if it arrived 200 ms earlier than the postsynaptic activation. Behavioral experiments proved that a CCKBR antagonist could block the generation of the visuo-auditory association, whereas a CCK agonist could rescue the defect association seen in $CCK^{-/-}$ mice.

Critical projections. Cross-modal association can be considered as the potentiation of synaptic strength between different modalities. Consistent with other studies(Bizley et al., 2007; Budinger et al., 2006; Falchier et al., 2002; Falchier et al., 2010; Rockland and Ojima, 2003), we describe a direct projection in the mouse from the VC to the AC for the visuo-auditory association using both retrograde and anterograde tracing methods. The projection terminates both in the superficial and deep cortical layers. Our previous study also on mouse demonstrated that neurons in the entorhinal cortex retrogradely labeled by true blue injected into the AC are almost 100% CCK^+ (Li et al., 2014). We here confirm that CCK also is expressed in neurons of the EC projection to the AC.

Cortical neuropeptides. Cortical neurons express a number of neuropeptides (Somogyi and Klausberger, 2005), whereby CCK is the most abundant of all. CCK comes in different forms, but it is the sulphated octapeptide, CCK-8S, that predominates in the brain (Dockray et al., 1978; Rehfeld, 1978). CCK is expressed in GABAergic interneurons (Houser et al., 1983), and many pyramidal neurons (DeFelipe and Fariñas, 1992) have also high levels of CCK transcript (Burgunder and Young, 1988; Schiffmann and Vanderhaeghen, 1991). The CCK^+ interneurons are relatively few, but exert a critical control of cortical activity (Somogyi and Klausberger, 2005). However, it is CCK in the pyramidal neurons that are in focus in the present study, especially the CCK^+, glutamatergic projection from EC to AC. We also use exogenous CCK in the experiments, both CCK-8S and CCK-4 which is the C-terminus not only of proCCK but also of gastrin. The small size of the latter fragment is the reason, why it is considered to pass the blood-brain-barrier (Rehfeld, 2000). However, we infused CCK-4 into the transverse venous sinus aiming at obtaining maximal peptide levels in the cortex.

Optogenetics. The present study is based on optogenetics, that is genetic introduction of light sensitive channels (Channelrodopsins), allowing control of selective neuron populations by light - a method that has revolutionized neuroscience research(Deisseroth et al., 2006; Knopfel et al., 2010). Here, using the two channels Chronos and ChrimsonR, we were able to activate two distinct projection terminals converging in the same target area activate (the EC→AC CCK^+ projection and the VC→AC projection).

Prerequisits for synaptic plasticity. Our previous finding based on in vivo intracellular recording indicated that there are three prerequisites to enable synaptic plasticity: presynaptic activation, postsynaptic firing, and, in this particular system, the presence of CCK(Li et al., 2014). Replacing the classical HFS protocol (HFLS of VC→AC projections) with local infusion of CCK-8S followed by pairing between pre-synaptic VC→AC inputs induced by VALS and postsynaptic firing evoked by noise stimuli led to the potentiation of VC→AC inputs. We hypothesize that these events may underlie the visuo-auditory association observed in the auditory cortex, further demonstrating the critical role of CCK to enable synaptic plasticity(Chen et al., 2019; Li et al., 2014).

Simple pairing between HFLS of EC→AC, CCK^+ projection and VALS without postsynaptic activation did not induce LTP in VC→AC inputs. Neither did low frequency (1 Hz) laser stimulation of the EC→AC CCK^+ projection induce LTP of VC→AC inputs, probably since no/not enough CCK was released by low frequency stimulation. Surprisingly, no LTP was recorded after HFLS of the VC→AC projection followed by Pre/Post Pairing. We demonstrate that VC→AC projecting neurons have relatively lower CCK expression compared to the EC→AC projecting neurons. This could be a reason why LTP was not observed for the VC→AC inputs after only 5 trails of HFLSVA/Pre/PostPairing. If the number of pairing trials or if laser stimulation intensity reaches a certain level, enough CCK may be released from the CCK^+ VC→AC projecting neurons, and LTP may occur.

These findings suggest that in traditional LTP HF stimulation also activates CCK^+ projection terminals, thereby releasing CCK and enabling potentiation (Chen et al., 2019). Subsequent experiments, in which the frequency of repetitive laser stimulation of EC→AC CCK^+ projection terminals was changed, showed that the degree of potentiation increased with increasing frequency. This finding can be explained by the frequency-dependent nature of

neuropeptide (CCK) release(Bean and Roth, 1991; Hökfelt, 1991; Iverfeldt et al., 1989; Shakiryanova et al., 2005; Whim and Lloyd, 1989).

In addition, the potentiation of VC→AC inputs decreased as the interval between the termination of HFLS and Pre/Post Pairing increased in the positive direction. A time window of 535 ms was observed to produce significant potentiation. If we would have increased the number of pairing trials, the effective Delay 1 might have lengthened.

Hebbian plasticity. We addressed the issue of spike timing-dependent plasticity and the critical time limit. Here the Hebbian rule has, arguably, been the most influential theory in learning and memory. This rule says that in order to induce potentiation the presynaptic subthreshold input should occur at most 20 ms before post-synaptic firing (Bi and Poo, 1998; Markram et al., 1997; Zhang et al., 1998). However, this theory has been challenged (Drew and Abbott, 2006; Izhikevich, 2007), with a prevalent question being: how can associations be established across behavioral time scales of seconds or even longer if the critical window is only 20 ms? (Bittner et al., 2017). Bittner et al. reported that five pairings of pre-synaptic subthreshold inputs with post-synaptic calcium plateau potentials produce a large potentiation; and that presynaptic inputs can arrive seconds before or after postsynaptic activity, a phenomenon termed "behavioral time scale synaptic plasticity" (Bittner et al., 2017).

This may account for the highly plastic nature of place fields in the hippocampus. In agreement, we observed potentiation in the neocortex, even when presynaptic input arrived 200 ms (Delay 2) earlier than postsynaptic firing and after only five trials pairing, but only in the presence of CCK. This time window could perhaps be extended as the paring trials increase. In general terms, these results fit with the fact that neuropeptides are known to exert slow and long-lasting effects (van den Pol, 2012). We did not explore the reverse direction, in which post-synaptic activity occurred before pre-synaptic activity, because noise stimuli induced more than one spike and thus timing would be difficult to control.

In summary, we found that a direct projection from the VC to the AC provide an anatomical basis for visuo-auditory association. The VC→AC inputs was potentiated after pairing with postsynaptic firing evoked by the auditory stimulus in the presence of CCK that was applied either exogenously or (endogenously) released from the EC→AC CCK^+ projection terminals stimulated with a HF laser. In the presence of endogenous CCK, significant potentiation of presynaptic input could be induced even it arrived 200 ms earlier than

postsynaptic firing and after only five trials of pairing. Finally, through the behavior experiments, we proved that the CCKBR antagonist blocked the establishment of visuo-auditory association, whereas the CCK agonist rescued the deficit of association in the $CCK^{-/-}$ mouse.

Materials and Methods

Animals

Adult male and female Sprague Dawley rats, C57BL/6J, CaMKIIa-Cre (Jackson lab stock #005359), Ai14 (Jackson lab stock #007914), and *CCK-ires-Cre* (Jackson lab stock #012706) mice were used in current study. For behavior experiments, only male animals were used. Animals were confirmed to have clean external ears and normal hearing and were housed in a 12-hour-light/12-hour-dark cycle (lights on from 8:00 pm to 8:00 am next day) at 20-24°C with 40-60% humidity with ad libitum access to food and water. All procedures were approved by the Animal Subjects Ethics Sub-Committees of City University of Hong Kong.

Anesthesia and surgery

To induce anesthesia for retrograde tracer or virus injection, animals were administered (i.p.) with 50 mg/kg pentobarbital (Dorminal 20%, Alfasan International B.V., Woerden, Netherlands). To induce anesthesia for acute *in vivo* recording, urethane sodium (2 g/kg, i.p., Sigma-Aldrich, St. Louis, MO, USA) was used with periodic supplements throughout surgery and neuronal recordings. During surgery, lidocaine (2%, Tokyo Chemical Industry [TCI] #L0156, Tokyo, Japan) was frequently applied in drops on the incision site. After confirming anesthesia, head fur between the eyes and ears was trimmed. Animals were mounted on a stereotaxic instrument (for rats, Narishige # SR-6R-HT, Japan; for mice, RWD Life Science # 68001, China). The scalp was sterilized with 70% ethanol. The body temperature was maintained at 37 – 38°C with a heating blanket (Homeothermic Blanket system, Harvard Apparatus, US) during surgery. After making a midline incision, muscle or periosteum was carefully removed with a scalpel blade. And after leveling, we made craniotomies over different target brain regions. All surgery tools were autoclaved before experiments. Before returning to the Laboratory Animal Research for normal holding, we monitored animals until they completely regained consciousness. To prevent infection, we applied erythromycin ointment to the wound for 7 days after surgery.

Retrograde tracing

For retrograde tracing on rat, a craniotomy window of 1.5 mm by 2.5 mm was made to access the auditory cortex at the left temporal bone, 3.0 to 4.5 mm from the top edge (dorsal-ventral, DV) and −3.0 to −5.5 mm from bregma (anterior-posterior, AP). CTB 488 (1 mg/mL, Molecular Probes #C34775, US) was injected into three locations with different coordinates (AP -3.5 mm, DV -3.8 mm; AP -4.5 mm, DV -3.8 mm; and AP-5.5, DV -3.8). For each location, two depths from the surface of the cortex were adopted (-500 μm and -900 μm, 50 nl each depth). After all injections, the craniotomy window was filled with Kwik-cast silicone gel (World Precision Instruments, US), and the incision was sutured. Animals were kept on the heating pad until voluntary movements, and then returned to their cages. Five days later, animals were transcardially perfused with PBS and 4% paraformaldehyde, sequentially.

in vivo fEPSP Recording with optogenetics

For dual pathways, we injected AAV9-Ef1α-Flex-Chronos-GFP (3.7 E+12 vg/mL, Boyden/UNC vector core) and AAV9-Syn-ChrimsonR-tdTomato (4.1 E+12 vg/mL, Boyden/UNC vector core) in the Ent and VC of CCK-ires-Cre mic*e* to separately activate auditory cortical projections from entorhinal and visual cortices respectively. We tried both the lateral (LENT, AP -4.2 mm, ML 3.5 mm and DV -3.0 mm [below the pia], 300 nl) and medial (MENT, AP -4.9 mm, ML 3.3 mm, DV -3.2, -2.5 and -1.8 mm [below the pia, 7^0 to the rostral direction], 100 nl each depth) part of Ent.. For the VC, to avoid the spread of virus directly into the auditory cortex, the medial part of the visual cortex was chosen as the target area. Two locations distributed rostro-caudally with different coordinates (AP -2.7 mm, ML 1.7 mm, DV -0.5 mm; AP -3.3 mm, ML 1.7 mm, DV -0.5 mm; 150 nl each depth) were adopted. Before the electrophysiological experiment, we waited for 4-5 weeks for the opsins to well expressed in the projection terminals. We adopted 473 nm and 635 nm lasers to stimulate the projection terminals in the auditory cortex from the entorhinal and visual cortices respectively and recorded the laser evoked fEPSP with glass pipette electrodes (~1M Ohm) rather than metal electrodes to prevent photoelectric artifacts. During recording, the optic fiber was positioned on the surface of the auditory cortex to illuminate the recording site. To examine the optimal laser intensity needed for separately activating the two channelrhodopsins, we injected AAV9-Ef1α-Flex-Chronos-GFP in the Ent (Figure S2A), or

AAV9-hSyn-ChrimsonR-tdTomato in the VC (Figure S2B) of the CCK-iRES-Cre mice. In the former, as shown in Figure S2A right, the fEPSP slopes gradually increased with increasing intensity of the 473 nm laser and became saturated at 30 mW/mm^2 (green solid). However, no responses were evoked by the 635-nm laser, even at an intensity of 40 mW/mm^2 (red dash). Conversely, in animal with injection of AAV9-hSyn-ChrimsonR-tdTomato in the VC the fEPSP slopes gradually increased and became saturated (red solid) with the 635 nm laser. However, here 40 mW (green dash) produced fEPSPs, but they were relatively small (Figure S2B right). Thus, to avoid cross talk we controlled the fiber end intensities of 473 nm and 635 nm laser below 30 and 40 mW/mm^2.

For single pathway (VC→AC) activation experiment, we injected AAV9-Ef1α-Flex-Chronos-GFP and AAV9-Syn-ChrimsonR-tdTomato in the VC of CaMKIIα-Cre and wildtype mice respectively. The coordinates are same as above.

Brain slice preparation and patch clamp recordings

At least four weeks after virus injection, acute brain slices were prepared using a protective cutting and recovery method to achieve a higher success rate for patch clamp. Briefly, anesthetized mice received transcardial perfusion with NMDG-aCSF (92 mM NMDG, 2.5 mM KCl, 1.25 mM NaH2PO4, 30 mM NaHCO3, 20 mM HEPES, 25 mM glucose, 2 mM thiourea, 5 mM Na-ascorbate, 3 mM Na-pyruvate, 0.5 mM CaCl2·4H2O and 10 mM MgSO4·7H2O; pH 7.3-7.4), and the brain was gently extracted from the skull and then cut into 300 μm thick sections. Slices were submerged in NMDG-aCSF for 5-10 min at 32-34 °C to allow protective recovery and then incubated at room-temperature ACSF (119 mM NaCl, 2.5 mM KCl, 1.25 mM NaH2PO4, 24 mM NaHCO3, 12.5 mM glucose, 2 mM CaCl2·4H2O and 2 mM MgSO4·7H2O, ~25 °C) for at least 1 h before transferring into recording chamber. All solutions were oxygenated with 95% O_2/5% CO_2 for 30 min in advance.

Whole-cell recordings were made from pyramidal neurons at the auditory cortex at room temperature. The signals were amplified with Multiclamp 700B amplifier, digitized with Digital 1440A digitizer and acquired at 20 kHz using Clampex 10.3 (Molecular Devices, Sunnyvale, CA). Patch pipettes with a resistance between 3-5 MΩ were pulled from borosilicate glass (WPI)

with a Sutter-87 puller (Sutter). The intracellular solution contained: 145 mM K-Gluconate, 10 mM HEPES, 1 mM EGTA, 2 mM MgATP, 0.3 mM Na2-GTP, and 2 mM MgCl2; pH 7.3; 290–300 mOsm. The pipette was back-filled with internal solution containing 145 mM K-Gluconate, 10 mM HEPES, 1 mM EGTA, 2 mM MgATP, 0.3 mM Na2-GTP, and 2 mM MgCl2; pH 7.3; 290–300 mOsm.

Pyramidal neurons were selected based on the pyramidal-like shape and the firing pattern of regular spiking by injecting a series of hyperpolarizing and depolarizing current with 50 pA increments (1s). An electrical stimulation electrode was placed ~200 μm from the recording neuron and laser stimulation were presented by using Aurora-220 (473 nm and 635 nm, NEWDOON) through an optic fiber. Only neurons that could be activated by laser stimulation and electrical stimulation were recruited in the following experiment. Under voltage-clamp recording mode (holding at -70 mV), EPSCs induced by electrical stimulation (0.05 Hz, 0.5 ms) and laser stimulation (0.05 Hz, 1-5 ms, 2mW) were stably recorded for 10 min. Then high frequency (60 Hz, 5 pulses, 1-5 ms duration, 2 mW) stimulation of CCK terminal or VC terminal was delivered, followed by the pairng of simultaneous VALS and ESAC. This stimulation protocol was repeated 5 times with a 10-s interval. Electrical stimulation induced EPSCs were then recorded for another 30 min. Intensities of electrical stimulation were adjusted to maintain the amplitude of EPSCs at around 200-300 pA. -5 mV hyperpolarizing pulses (10 ms) were applied every 20s to measure access resistance (Ra) throughout whole recording procedure and recordings were terminated if Ra changed more than 20%.

Quantification of CCK expression levels of AC projecting neurons in the VC and the Ent

AAVretro-Cre (pENN-AAV/retro-hSyn-Cre-WPRE-hGH, 2.10E+13 vg/mL, Addgene, USA) was injected in three locations (100 nl/each) of the left AC of the Ai14 mice. The coordinates were as follows: AP -2.6 mm (site 1) or -2.9 mm (site 2) or -3.2 mm (site 3), ML 1.0 mm ventral to the edge differentiating the parietal and temporal skull, and DV -0.5 mm from the dura. Three weeks later, the mice were deeply anesthetized with pentobarbital (Dorminal 20%, Alfasan International B.V., Woerden, Netherlands) and transcardially perfused with 20 ml of warm (37°C) 0.9% saline, 20 ml of warm fixative (4% paraformaldehyde, 0.4% picric acid, 0.1% glutaraldehyde in PBS) and 20 ml of the same ice-cold fixative. Brains were dissected out and

post-fixed in the same fixative for 24h at 4°C. The tissues were then washed 3 times with PBS and cryoprotected in 10% [over night (O/N) at 4°C), 20% (O/N at 4°C) and 30% (O/N at 4°C) sucrose in PBS. Tissues were embedded in OCT compound, sectioned at 20 µm, and mounted onto Superfrost plus slides (Thermo Fischer Scientific, Waltham, MA). For in situ hybridization (RNAscope), the manufacturer's protocol was followed (Advanced Cell Diagnostics, San Francisco, CA). All experiments were replicated in three animals. The probes were designed by the manufacture and available from Advanced Cell Diagnostics. The following probes were used in this study: Mm-Slc17a7- C2 (#416631-C2), Mm-Cck-C1 (#402271-C1), Mm-Tomato-C4 (#317041-C4). Methods of counting and quantifying the cells, and criteria of high level Cck epression. For each animal, Cck expression level was normalized to the average Cck expression in projecting neurons in visual cortex. Neurons expressing low Cck (below the average of Cck expression among projecting neurons in visual cortex) are indicated in grey.

Associative learning test after CCKBR antagonist application in the AC.

After the same anesthesia and surgery as mentioned earlier, a drug infusion cannula was implanted in each hemisphere of the AC of the C57 mouse. The mouse was allowed for recovery for 2 days. For the experimental group, the VS and AS were first presented in pairs to the mouse for 25 trials in each session after the auditory cortex was bilaterally infused with CCKB receptor (CCKBR) antagonist (L365, 260, 10µM in 2% DMSO-ACSF, 0.5µl in both sides, injection speed 0.05µL/min), and for 4 sessions each day during 3 days. For the control group, CCKBR antagonist was replaced with ACSF. On day 4, a baseline test for the percentage of freezing over a time period of 10s was carried out after the VS and AS were presented separately. The AS was then conditioned with footshock for 3 trials. On day 5, post-conditioning tests were carried out to the VS and AS separately. The freezing percentages of different groups to VS were compared by two-way ANOVA.

Associative learning test after CCK-4 administration in CCK$^{-/-}$ Mice.

A drug infusion cannula was implanted on the top of the venous sinus (transverse sinus) of the CCK$^{-/-}$ mouse to administer drugs though i.v. injection. After the i.v. injection of CCK4 (0.01ml, 3.4µM; 1ug/kg) or saline (0.01ml), the VS and AS were immediately presented in pairs to the mouse for 25 trials in each session for 4 sessions each day for 3 consecutive days. The rest of the

626 procedure was the same as the previous experiment. To induce a similar percentage of freezing
627 of C57 mice, the CCK$^{-/-}$ mice needed 9 trials. In a separate experiment to test the dosage of CCK4
628 that induced panic attack or anxiety, different dosage of CCK4 (2.5, 25 and 250 ug/kg) or vehicle
629 (saline with 5% DMSO) was injected intraperitoneally and the mice activities were monitored
630 for up to 60 minutes after injection. Activities of mice were normalized to the average activities
631 of the vehicle group.

632 ***Histology***

633 After completing all experiments, animal was anesthetized with an overdose of pentobarbital and
634 transcardially perfused with PBS and 4% paraformaldehyde sequentially. Brains were then
635 collected and post-fixed in 4% paraformaldehyde for 24 h. A vibrating blade microtome (VT
636 1000s, Leica, Germany) was used to cut the brain tissue into sections (60 μm thick). Nissl
637 (Neurotrace 640, 1:200 in 0.01 M PBS with 0.1% Triton X-100, 2h, Thermo Fisher Scientific
638 #N21483, Waltham, MA, USA) or DAPI (1:10000 in 0.01 M PBS, 10 min, Santa Cruz
639 Biotechnology #sc-3598, Dallas, TX, USA) staining was performed in some experiments.
640 Images were obtained with a Nikon Eclipse Ni-E upright fluorescence microscope (Tokyo, Japan)
641 or a Zeiss LSM880 confocal microscope (Oberkochen, Germany).

642 ***Acoustic stimuli, visual stimuli, electrical stimulation, and laser stimulation***

643 All stimuli were generated from computer-controlled RZ6 and RZ5D integrated stimulation
644 stations (Tucker-Davis Technologies [TDT], FL, USA) controlled by self-coded OpenEX
645 program (TDT, FL, USA). Acoustic stimuli were generated as analogue signals and delivered
646 through a close-field speaker (MF1, TDT). The sound pressure level of acoustic stimuli was
647 controlled with OpenEx program and calibrated with a condenser microphone (Center
648 Technology, Taipei). Visual stimuli were generated as analogue signals and delivered though the
649 white LED array. Lasers with wavelengths of 473 nm and 635 nm were generated from different
650 laser generators (Intelligent optogenetic system, Newdoon, China), and 561 nm laser was
651 generated from a separate laser generator (New Industries Optoelectronics Tech Co., China). All
652 lasers were controlled by analogue signals from TDT system. The single pulse width of the laser
653 was always 5 ms.

Data acquisition and analysis

All *in vivo* electrophysiological data were recorded through TDT system which was controlled by self-coded program in OpenEX (TDT, FL, USA). The filters for spikes and local field potential recordings were set as 500-3,000 Hz and 1-500 Hz, respectively. To identify spikes, the threshold was set as three times the standard deviation of baseline. Offline Sorter (Plexon Inc, US) was used to perform spike sorting, and NeuroExplorer Version 5 (Nex Technologies, US) was used to perform further single unit analysis. Custom Matlab (Mathworks Inc., US) program was used to analyze the recorded fEPSPs. We only included the recording sites in the in vivo or cells in the in vitro experiments with a stable baseline recording. To compare the changes in fEPSP slopes or EPSC amplitudes, the mean of baseline values was first calculated, to which all the slopes or amplitudes were normalized, respectively. For in vivo recording, normalized fEPSP slopes of the last 10 data points (each data point was averaged from the slopes of 6 fEPSPs evoked by VALS, AS or EALS) from baseline and post-pairing test sessions were chosen and averaged to obtain pairs of before and after values for each recording site to perform statistical test. For in vitro patch recording, each data point was averaged from the amplitudes of 3 consecutive EPSCs evoked by VALS or ESAC. And for each cell, the average of 10 baseline data points and the average of last 8 data points of the post-paring session were chosen to generate the pairs of before and after values to perform statistical test. All statistical analyses (paired t-tests, unpaired t-test or two-way RM ANOVA) were performed using SPSS software (IBM, US). Pairwise comparisons were adjusted by Bonferroni correction. Statistical significance was set at $p < 0.05$.

Acknowledgements

This work was supported by: Hong Kong Research Grants Council, General Research Fund: 11103220M, 11101521M (GRF, JFH); Hong Kong Research Grants Council, Collaborative Research Fund: C1043-21GF(CRF, JFH); Innovation and Technology Fund: MRP/053/18X, GHP_075_19GD (ITF, JFH); Health and Medical Research Fund: 06172456, 09203656 (HMRF, XC, JFH); The Swedish Research Council: 2018-0273 (TH); The Arvid Carlsson Foundation (TH); The Swedish Research Council: 220-01688 (TH); Key-Area Research and Development Program of Guangdong Province: 2018B030340001(WJS); and the following charitable

684 foundations for their generous support to JFH: Wong Chun Hong Endowed Chair Professorship,
685 Charlie Lee Charitable Foundation, and Fong Shu Fook Tong Foundation.
686

687 **Author Contributions**

688 WJS, XC, JFS, TH, and JFH designed the experiments; WJS, YJP, XC and YL collected and
689 analyzed the data of the physiological part; HHW and MZ collected and analyzed the RNAscope
690 data; YJP, XJZ and HMF collected and analyzed the data of the behavioral part; WJS, PT, HL
691 and JL performed viral injection, retrograde tracing, and IHC experiments; WJS, XC, TH and
692 JFH wrote the manuscript.

693

694 **Declaration of Interests**

695 The authors declare no competing interests.

Reference

Bashir, Z.I., Alford, S., Davies, S.N., Randall, A.D., and Collingridge, G.L. (1991). Long-term potentiation of NMDA receptor-mediated synaptic transmission in the hippocampus. Nature *349*, 156-158.10.1038/349156a0

Bean, A.J., and Roth, R.H. (1991). Extracellular dopamine and neurotensin in rat prefrontal cortex in vivo: effects of median forebrain bundle stimulation frequency, stimulation pattern, and dopamine autoreceptors. The Journal of neuroscience : the official journal of the Society for Neuroscience *11*, 2694-2702

Beinfeld, M.C., Meyer, D.K., Eskay, R.L., Jensen, R.T., and Brownstein, M.J. (1981). The distribution of cholecystokinin immunoreactivity in the central nervous system of the rat as determined by radioimmunoassay. Brain research *212*, 51-57.10.1016/0006-8993(81)90031-7

Bi, G.Q., and Poo, M.M. (1998). Synaptic modifications in cultured hippocampal neurons: dependence on spike timing, synaptic strength, and postsynaptic cell type. The Journal of neuroscience : the official journal of the Society for Neuroscience *18*, 10464-10472

Bittner, K.C., Milstein, A.D., Grienberger, C., Romani, S., and Magee, J.C. (2017). Behavioral time scale synaptic plasticity underlies CA1 place fields. Science (New York, NY) *357*, 1033-1036.10.1126/science.aan3846

Bizley, J.K., Nodal, F.R., Bajo, V.M., Nelken, I., and King, A.J. (2007). Physiological and anatomical evidence for multisensory interactions in auditory cortex. Cerebral cortex (New York, NY : 1991) *17*, 2172-2189.10.1093/cercor/bhl128

Bliss, T.V., and Gardner-Medwin, A.R. (1973). Long-lasting potentiation of synaptic transmission in the dentate area of the unanaestetized rabbit following stimulation of the perforant path. The Journal of physiology *232*, 357-374.10.1113/jphysiol.1973.sp010274

Bliss, T.V., and Lomo, T. (1973). Long-lasting potentiation of synaptic transmission in the dentate area of the anaesthetized rabbit following stimulation of the perforant path. The Journal of physiology *232*, 331-356.10.1113/jphysiol.1973.sp010273

Brosch, M., Selezneva, E., and Scheich, H. (2005). Nonauditory events of a behavioral procedure activate auditory cortex of highly trained monkeys. The Journal of neuroscience : the official journal of the Society for Neuroscience *25*, 6797-6806.10.1523/jneurosci.1571-05.2005

725 Budinger, E., Heil, P., Hess, A., and Scheich, H. (2006). Multisensory processing via early
726 cortical stages: Connections of the primary auditory cortical field with other sensory systems.
727 Neuroscience *143*, 1065-1083.10.1016/j.neuroscience.2006.08.035
728 Burgunder, J.M., and Young, W.S. (1988). The distribution of thalamic projection neurons
729 containing cholecystokinin messenger RNA, using in situ hybridization histochemistry and
730 retrograde labeling. Brain research *464*, 179-189.10.1016/0169-328x(88)90024-1
731 Calvert, G.A., Bullmore, E.T., Brammer, M.J., Campbell, R., Williams, S.C., McGuire, P.K.,
732 Woodruff, P.W., Iversen, S.D., and David, A.S. (1997). Activation of auditory cortex during
733 silent lipreading. Science (New York, NY) *276*, 593-596.10.1126/science.276.5312.593
734 Canto, C.B., Wouterlood, F.G., and Witter, M.P. (2008). What does the anatomical organization
735 of the entorhinal cortex tell us? Neural plasticity *2008*, 381243.10.1155/2008/381243
736 Caporale, N., and Dan, Y. (2008). Spike timing-dependent plasticity: a Hebbian learning rule.
737 Annual review of neuroscience *31*, 25-46.10.1146/annurev.neuro.31.060407.125639
738 Cardin, J.A., Carlén, M., Meletis, K., Knoblich, U., Zhang, F., Deisseroth, K., Tsai, L.-H., and
739 Moore, C.I. (2010). Targeted optogenetic stimulation and recording of neurons in vivo using
740 cell-type-specific expression of Channelrhodopsin-2. Nature protocols *5*, 247-
741 254.10.1038/nprot.2009.228
742 Chen, X., Guo, Y., Feng, J., Liao, Z., Li, X., Wang, H., Li, X., and He, J. (2013). Encoding and
743 retrieval of artificial visuoauditory memory traces in the auditory cortex requires the entorhinal
744 cortex. The Journal of neuroscience : the official journal of the Society for Neuroscience *33*,
745 9963-9974.10.1523/jneurosci.4078-12.2013
746 Chen, X., Li, X., Wong, Y.T., Zheng, X., Wang, H., Peng, Y., Feng, H., Feng, J., Baibado, J.T.,
747 Jesky, R.*, et al.* (2019). Cholecystokinin release triggered by NMDA receptors produces LTP
748 and sound-sound associative memory. Proceedings of the National Academy of Sciences of the
749 United States of America *116*, 6397-6406.10.1073/pnas.1816833116
750 Cusick, C.G., Seltzer, B., Cola, M., and Griggs, E. (1995). Chemoarchitectonics and
751 corticocortical terminations within the superior temporal sulcus of the rhesus monkey: evidence
752 for subdivisions of superior temporal polysensory cortex. The Journal of comparative neurology
753 *360*, 513-535.10.1002/cne.903600312

754 DeFelipe, J., and Fariñas, I. (1992). The pyramidal neuron of the cerebral cortex: morphological
755 and chemical characteristics of the synaptic inputs. Progress in neurobiology *39*, 563-
756 607.10.1016/0301-0082(92)90015-7
757 Deisseroth, K., Feng, G., Majewska, A.K., Miesenböck, G., Ting, A., and Schnitzer, M.J. (2006).
758 Next-generation optical technologies for illuminating genetically targeted brain circuits. The
759 Journal of neuroscience : the official journal of the Society for Neuroscience *26*, 10380-
760 10386.10.1523/jneurosci.3863-06.2006
761 Dockray, G.J., Gregory, R.A., Hutchison, J.B., Harris, J.I., and Runswick, M.J. (1978). Isolation,
762 structure and biological activity of two cholecystokinin octapeptides from sheep brain. Nature
763 *274*, 711-713.10.1038/274711a0
764 Dodd, J., and Kelly, J.S. (1981). The actions of cholecystokinin and related peptides on
765 pyramidal neurones of the mammalian hippocampus. Brain research *205*, 337-
766 350.10.1016/0006-8993(81)90344-9
767 Drew, P.J., and Abbott, L.F. (2006). Extending the effects of spike-timing-dependent plasticity to
768 behavioral timescales. Proceedings of the National Academy of Sciences of the United States of
769 America *103*, 8876-8881.10.1073/pnas.0600676103
770 Falchier, A., Clavagnier, S., Barone, P., and Kennedy, H. (2002). Anatomical evidence of
771 multimodal integration in primate striate cortex. The Journal of neuroscience : the official journal
772 of the Society for Neuroscience *22*, 5749-5759
773 Falchier, A., Schroeder, C.E., Hackett, T.A., Lakatos, P., Nascimento-Silva, S., Ulbert, I.,
774 Karmos, G., and Smiley, J.F. (2010). Projection from visual areas V2 and prostriata to caudal
775 auditory cortex in the monkey. Cerebral cortex (New York, NY : 1991) *20*, 1529-
776 1538.10.1093/cercor/bhp213
777 Finney, E.M., Fine, I., and Dobkins, K.R. (2001). Visual stimuli activate auditory cortex in the
778 deaf. Nature neuroscience *4*, 1171-1173.10.1038/nn763
779 Foxe, J.J., Wylie, G.R., Martinez, A., Schroeder, C.E., Javitt, D.C., Guilfoyle, D., Ritter, W., and
780 Murray, M.M. (2002). Auditory-somatosensory multisensory processing in auditory association
781 cortex: an fMRI study. Journal of neurophysiology *88*, 540-543.10.1152/jn.2002.88.1.540
782 Fuster, J.M., Bodner, M., and Kroger, J.K. (2000). Cross-modal and cross-temporal association
783 in neurons of frontal cortex. Nature *405*, 347-351.10.1038/35012613

784 Greenwood, R.S., Godar, S.E., Reaves, T.A., Jr., and Hayward, J.N. (1981). Cholecystokinin in
785 hippocampal pathways. J Comp Neurol *203*, 335-350.10.1002/cne.902030303
786 Hendry, S.H., Jones, E.G., DeFelipe, J., Schmechel, D., Brandon, C., and Emson, P.C. (1984).
787 Neuropeptide-containing neurons of the cerebral cortex are also GABAergic. Proceedings of the
788 National Academy of Sciences of the United States of America *81*, 6526-
789 6530.10.1073/pnas.81.20.6526
790 Hernandez, R.V., Navarro, M.M., Rodriguez, W.A., Martinez, J.L., and LeBaron, R.G. (2005).
791 Differences in the magnitude of long-term potentiation produced by theta burst and high
792 frequency stimulation protocols matched in stimulus number. Brain research Brain research
793 protocols *15*, 6-13.10.1016/j.brainresprot.2005.02.003
794 Hökfelt, T. (1991). Neuropeptides in perspective: the last ten years. Neuron *7*, 867-
795 879.10.1016/0896-6273(91)90333-u
796 Horinouchi, Y., Akiyoshi, J., Nagata, A., Matsushita, H., Tsutsumi, T., Isogawa, K., Noda, T.,
797 and Nagayama, H. (2004). Reduced anxious behavior in mice lacking the CCK2 receptor gene.
798 European neuropsychopharmacology : the journal of the European College of
799 Neuropsychopharmacology *14*, 157-161.10.1016/S0924-977X(03)00103-2
800 Houser, C.R., Hendry, S.H., Jones, E.G., and Vaughn, J.E. (1983). Morphological diversity of
801 immunocytochemically identified GABA neurons in the monkey sensory-motor cortex. Journal
802 of neurocytology *12*, 617-638.10.1007/bf01181527
803 Innis, R.B., Corrêa, F.M., Uhl, G.R., Schneider, B., and Snyder, S.H. (1979). Cholecystokinin
804 octapeptide-like immunoreactivity: histochemical localization in rat brain. Proceedings of the
805 National Academy of Sciences of the United States of America *76*, 521-
806 525.10.1073/pnas.76.1.521
807 Iverfeldt, K., Serfözö, P., Diaz Arnesto, L., and Bartfai, T. (1989). Differential release of
808 coexisting neurotransmitters: frequency dependence of the efflux of substance P, thyrotropin
809 releasing hormone and 3Hserotonin from tissue slices of rat ventral spinal cord. Acta
810 physiologica Scandinavica *137*, 63-71.10.1111/j.1748-1716.1989.tb08721.x
811 Izhikevich, E.M. (2007). Solving the distal reward problem through linkage of STDP and
812 dopamine signaling. Cerebral cortex (New York, NY : 1991) *17*, 2443-
813 2452.10.1093/cercor/bhl152

814 Klapoetke, N.C., Murata, Y., Kim, S.S., Pulver, S.R., Birdsey-Benson, A., Cho, Y.K., Morimoto,
815 T.K., Chuong, A.S., Carpenter, E.J., Tian, Z., *et al.* (2014). Independent optical excitation of
816 distinct neural populations. Nature methods *11*, 338-346.10.1038/nmeth.2836
817 Knopfel, T., Lin, M.Z., Levskaya, A., Tian, L., Lin, J.Y., and Boyden, E.S. (2010). Toward the
818 second generation of optogenetic tools. The Journal of neuroscience : the official journal of the
819 Society for Neuroscience *30*, 14998-15004.10.1523/JNEUROSCI.4190-10.2010
820 Kohler, C., and Chan-Palay, V. (1982). The distribution of cholecystokinin-like immunoreactive
821 neurons and nerve terminals in the retrohippocampal region in the rat and guinea pig. J Comp
822 Neurol *210*, 136-146.10.1002/cne.902100204
823 Kozai, T.D.Y., and Vazquez, A.L. (2015). Photoelectric artefact from optogenetics and imaging
824 on microelectrodes and bioelectronics: New Challenges and Opportunities. Journal of materials
825 chemistry B *3*, 4965-4978.10.1039/c5tb00108k
826 Larsson, L., and Rehfeld, J.F. (1979). A peptide resembling COOH-terminal tetrapeptide amide
827 of gastrin from a new gastrointestinal endocrine cell type. Nature *277*, 575-
828 578.10.1038/277575a0
829 Li, X., Yu, K., Zhang, Z., Sun, W., Yang, Z., Feng, J., Chen, X., Liu, C.-H., Wang, H., Guo, Y.P.,
830 *et al.* (2014). Cholecystokinin from the entorhinal cortex enables neural plasticity in the auditory
831 cortex. Cell research *24*, 307-330.10.1038/cr.2013.164
832 Lipton, P.A., Alvarez, P., and Eichenbaum, H. (1999). Crossmodal associative memory
833 representations in rodent orbitofrontal cortex. Neuron *22*, 349-359.10.1016/s0896-
834 6273(00)81095-8
835 Lo, C.-M., Samuelson, L.C., Chambers, J.B., King, A., Heiman, J., Jandacek, R.J., Sakai, R.R.,
836 Benoit, S.C., Raybould, H.E., Woods, S.C., *et al.* (2008). Characterization of mice lacking the
837 gene for cholecystokinin. American journal of physiology Regulatory, integrative and
838 comparative physiology *294*, R803-810.10.1152/ajpregu.00682.2007
839 Löwel, S., and Singer, W. (1992). Selection of intrinsic horizontal connections in the visual
840 cortex by correlated neuronal activity. Science (New York, NY) *255*, 209-
841 212.10.1126/science.1372754
842 Lundberg, J.M., and Hokfelt, T. (1983). Coexistence of peptides and classical neurotransmitters.
843 Trends in Neurosciences *6*, 325-333.10.1016/0166-2236(83)90149-2

844 Markram, H., Lübke, J., Frotscher, M., and Sakmann, B. (1997). Regulation of synaptic efficacy
845 by coincidence of postsynaptic APs and EPSPs. Science (New York, NY) *275*, 213-
846 215.10.1126/science.275.5297.213
847 Meziane, H., Devigne, C., Tramu, G., and Soumireu-Mourat, B. (1993). Effects of anti-CCK-8
848 antiserum on acquisition and retrieval by mice in an appetitive task. Peptides *14*, 67-
849 73.10.1016/0196-9781(93)90012-6
850 Meziane, H., Devigne, C., Tramu, G., and Soumireu-Mourat, B. (1997). Distribution of
851 cholecystokinin immunoreactivity in the BALB/c mouse forebrain: an immunocytochemical
852 study. Journal of chemical neuroanatomy *12*, 191-209.10.1016/s0891-0618(96)00211-6
853 Milner, B., and Klein, D. (2016). Loss of recent memory after bilateral hippocampal lesions:
854 memory and memories-looking back and looking forward. Journal of neurology, neurosurgery,
855 and psychiatry *87*, 230.10.1136/jnnp-2015-311092
856 Nomoto, S., Miyake, M., Ohta, M., Funakoshi, A., and Miyasaka, K. (1999). Impaired learning
857 and memory in OLETF rats without cholecystokinin (CCK)-A receptor. Physiology & behavior
858 *66*, 869-872.10.1016/s0031-9384(99)00033-5
859 Pekkola, J., Ojanen, V., Autti, T., Jääskeläinen, I.P., Möttönen, R., and Sams, M. (2006).
860 Attention to visual speech gestures enhances hemodynamic activity in the left planum temporale.
861 Human brain mapping *27*, 471-477.10.1002/hbm.20190
862 Rehfeld, J.F. (1978). Immunochemical studies on cholecystokinin. II. Distribution and molecular
863 heterogeneity in the central nervous system and small intestine of man and hog. The Journal of
864 biological chemistry *253*, 4022-4030
865 Rehfeld, J.F. (2000). Cholecystokinin and panic disorder--three unsettled questions. Regulatory
866 peptides *93*, 79-83.10.1016/s0167-0115(00)00179-8
867 Rockland, K.S., and Ojima, H. (2003). Multisensory convergence in calcarine visual areas in
868 macaque monkey. International journal of psychophysiology : official journal of the International
869 Organization of Psychophysiology *50*, 19-26.10.1016/s0167-8760(03)00121-1
870 Sakai, K., and Miyashita, Y. (1991). Neural organization for the long-term memory of paired
871 associates. Nature *354*, 152-155.10.1038/354152a0
872 Schiffmann, S.N., and Vanderhaeghen, J.J. (1991). Distribution of cells containing mRNA
873 encoding cholecystokinin in the rat central nervous system. The Journal of comparative
874 neurology *304*, 219-233.10.1002/cne.903040206

875 Schlack, A., Sterbing-D'Angelo, S.J., Hartung, K., Hoffmann, K.-P., and Bremmer, F. (2005).
876 Multisensory space representations in the macaque ventral intraparietal area. The Journal of
877 neuroscience : the official journal of the Society for Neuroscience *25*, 4616-
878 4625.10.1523/jneurosci.0455-05.2005
879 Scoville, W.B., and Milner, B. (1957). Loss of recent memory after bilateral hippocampal lesions.
880 Journal of neurology, neurosurgery, and psychiatry *20*, 11-21.10.1136/jnnp.20.1.11
881 Seltzer, B., Cola, M.G., Gutierrez, C., Massee, M., Weldon, C., and Cusick, C.G. (1996).
882 Overlapping and nonoverlapping cortical projections to cortex of the superior temporal sulcus in
883 the rhesus monkey: double anterograde tracer studies. The Journal of comparative neurology *370*,
884 173-190.10.1002/(sici)1096-9861(19960624)370:2<173::aid-cne4>3.0.co;2-#
885 Shakiryanova, D., Tully, A., Hewes, R.S., Deitcher, D.L., and Levitan, E.S. (2005). Activity-
886 dependent liberation of synaptic neuropeptide vesicles. Nature neuroscience *8*, 173-
887 178.10.1038/nn1377
888 Siegel, R.E., and Young, W.S. (1985). Detection of preprocholecystokinin and preproenkephalin
889 A mRNAs in rat brain by hybridization histochemistry using complementary RNA probes.
890 Neuropeptides *6*, 573-580.10.1016/0143-4179(85)90121-0
891 Somogyi, P., Hodgson, A.J., Smith, A.D., Nunzi, M.G., Gorio, A., and Wu, J.Y. (1984).
892 Different populations of GABAergic neurons in the visual cortex and hippocampus of cat
893 contain somatostatin- or cholecystokinin-immunoreactive material. The Journal of neuroscience :
894 the official journal of the Society for Neuroscience *4*, 2590-2603
895 Somogyi, P., and Klausberger, T. (2005). Defined types of cortical interneurone structure space
896 and spike timing in the hippocampus. The Journal of physiology *562*, 9-
897 26.10.1113/jphysiol.2004.078915
898 Sugihara, T., Diltz, M.D., Averbeck, B.B., and Romanski, L.M. (2006). Integration of auditory
899 and visual communication information in the primate ventrolateral prefrontal cortex. The Journal
900 of neuroscience : the official journal of the Society for Neuroscience *26*, 11138-
901 11147.10.1523/jneurosci.3550-06.2006
902 Swanson, L.W., and Köhler, C. (1986). Anatomical evidence for direct projections from the
903 entorhinal area to the entire cortical mantle in the rat. The Journal of neuroscience : the official
904 journal of the Society for Neuroscience *6*, 3010-3023

905 Tsutsumi, T., Akiyoshi, J., Isogawa, K., Kohno, Y., Hikichi, T., and Nagayama, H. (1999).
906 Suppression of conditioned fear by administration of CCKB receptor antagonist PD135158.
907 Neuropeptides *33*, 483-486.10.1054/npep.1999.0766
908 van den Pol, A.N. (2012). Neuropeptide transmission in brain circuits. Neuron *76*, 98-
909 115.10.1016/j.neuron.2012.09.014
910 Vanderhaeghen, J.J., Lotstra, F., Mey, J., and Gilles, C. (1980). Immunohistochemical
911 localization of cholecystokinin- and gastrin-like peptides in the brain and hypophysis of the rat.
912 Proceedings of the National Academy of Sciences of the United States of America *77*, 1190-
913 1194.10.1073/pnas.77.2.1190
914 Whim, M.D., and Lloyd, P.E. (1989). Frequency-dependent release of peptide cotransmitters
915 from identified cholinergic motor neurons in Aplysia. Proceedings of the National Academy of
916 Sciences of the United States of America *86*, 9034-9038.10.1073/pnas.86.22.9034
917 Yun, S.H., Mook-Jung, I., and Jung, M.W. (2002). Variation in effective stimulus patterns for
918 induction of long-term potentiation across different layers of rat entorhinal cortex. The Journal of
919 neuroscience : the official journal of the Society for Neuroscience *22*, RC214
920 Zhang, L.I., Tao, H.W., Holt, C.E., Harris, W.A., and Poo, M. (1998). A critical window for
921 cooperation and competition among developing retinotectal synapses. Nature *395*, 37-
922 44.10.1038/25665
923 Zhang, Z., Zheng, X., Sun, W., Peng, Y., Guo, Y., Lu, D., Zheng, Y., Li, X., Jendrichovsky, P.,
924 Tang, P.*, et al.* (2020). Visuoauditory Associative Memory Established with Cholecystokinin
925 Under Anesthesia Is Retrieved in Behavioral Contexts. The Journal of neuroscience : the official
926 journal of the Society for Neuroscience *40*, 2025-2037.10.1523/jneurosci.1673-19.2019
927 Zhou, Y.-D., and Fuster, J.M. (2004). Somatosensory cell response to an auditory cue in a haptic
928 memory task. Behavioural brain research *153*, 573-578.10.1016/j.bbr.2003.12.024
929 Zhou, Y.D., and Fuster, J.M. (2000). Visuo-tactile cross-modal associations in cortical
930 somatosensory cells. Proceedings of the National Academy of Sciences of the United States of
931 America *97*, 9777-9782.10.1073/pnas.97.17.9777

932

933

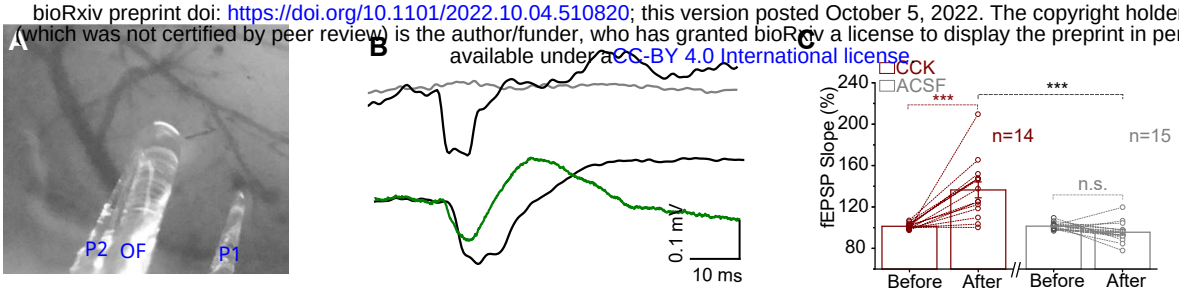

Supplementary Figure 1.

(A) An example image of the positions of glass pipette recording electrodes (P1 and P2) and optical fiber (OF) for laser stimulation.

(B) Upper: example fEPSP traces recorded by glass (Gray) or tungsten (black, artefact) electrode in wild type mice without any expression in the recording site. Bottom, example fEPSP traces recorded by glass (green, real signal) or tungsten (black, mixture of artefact and true signal) electrodes in the Cck-iRES-Cre mice with the expression of ChR2 in the projecting terminals of the recording area.

(C) Individual and average fEPSPVALS slope changes before and after Pre/Post Pairing with CCK-8S (red) or ACSF (gray) infusion in the AC. *** $p < 0.001$, n.s. $p = 0.411$, $n = 14$ for CCK group, $n = 15$ for ACSF group, two-way RM ANOVA with post-hoc Bonferroni test.

See Table S1 for detailed Statistics.

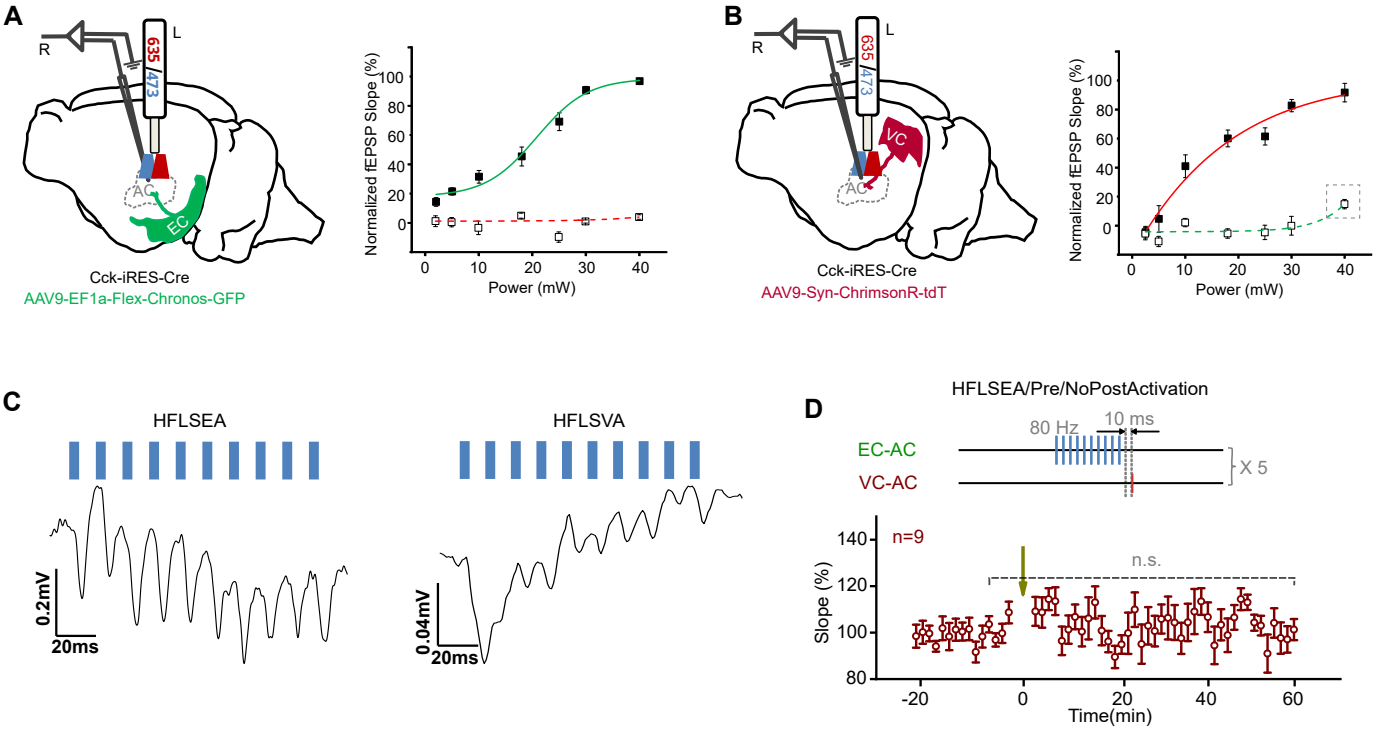

Supplementary Figure 2.

(A) and (B) Optimal laser power determination of 473 nm and 635 nm to prevent crosstalk. Diagram of the experimental design, animals with only one injection of either AAV9-Ef1α-Flex-Chronos-GFP into the entorhinal cortex (A left) or AAV9-Syn-ChrimsonR-tdTomato into the visual cortex (B left) were prepared, 473 nm and 635 nm were both applied to stimulate their terminals in the auditory cortex, and their corresponding local field potentials were recorded by glass pipette electrodes. A right, normalized fEPSPs slopes (n=9) evoked by 473 nm (green line) or 635 nm (red dashed line) laser stimulation of CCK+ ENT→AC projection terminals; B right, normalized fEPSPs slopes (n=12) evoked by 473 nm (green dashed line) or 635 nm (red solid line) laser stimulation of VC→AC universal projection terminals; gray dashed rectangle in B-right emphasizes the power that may induce crosstalk.

(C) Example traces of HFLSEA (left) and HFLSVA (right). Scale bars: left, 20 ms and 0.2 mV; right, 20 ms and 0.04 mV.

(D) Upper: schematic drawing of the protocol of HFLSEA/Pre/NoPostActivation. Bottom: normalized fEPSPVALS slopes before and after HFLSEA/Pre/NoPostActivation. Error bars represent SEM. paired t-test, t (8) = -0.899, n.s. p = 0.395, n = 9.

See Table S1 for detailed Statistics.

S-Fig.3

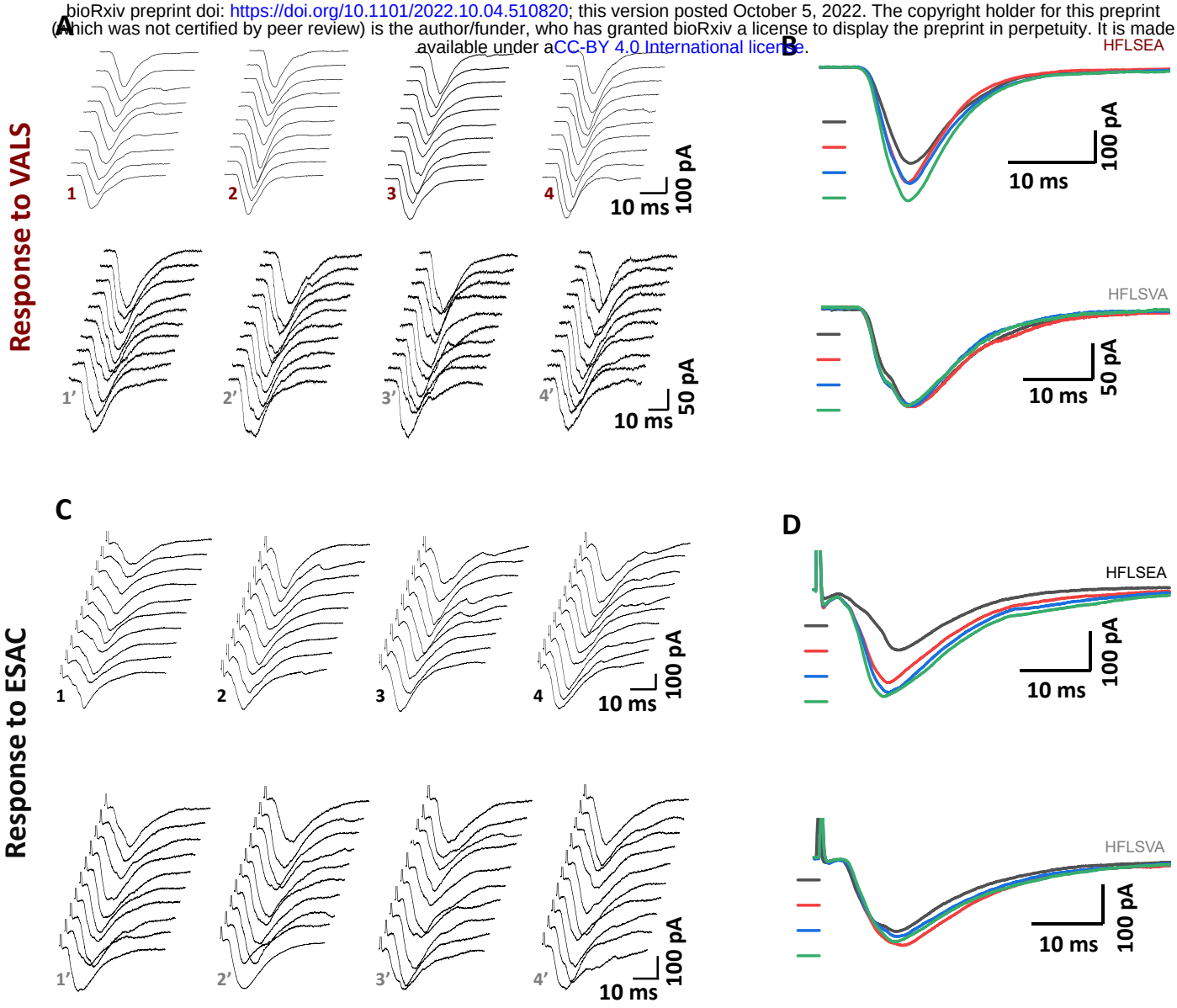

Supplementary Figure 3.

(A) Representative EPSCVALS traces at different timepoints and (B) their averaged traces in the HFLSEA/Pre/PostPairing (upper) or HFLSVA/Pre/PostPairing (bottom) group. (1 or 1': first 10 consecutive individual trace before pairing; 2-4 or 2'-4': 10 consecutive individual trace 0 min, 13 min and 27 min after pairing respectively).

(C) Representative EPSCESAC traces at different timepoints and (D) their averaged traces in the HFLSEA/Pre/PostPairing (upper) or HFLSVA/Pre/PostPairing (bottom) group. (1 or 1': first 10 consecutive individual trace before pairing; 2-4 or 2'-4': 10 consecutive individual trace 0 min, 13 min and 27 min after pairing respectively).

See Table S1 for detailed Statistics.

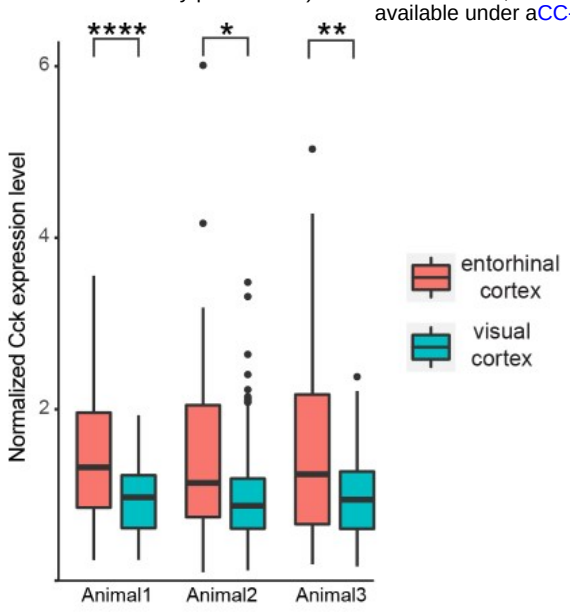

Supplementary Figure 4.

Comparison of Cck expression level in neurons in the Ent and VC which project to the VC. For each animal, Cck expression level is normalized to the average Cck expression in projecting neurons in visual cortex. Unpaired t-test, ****p<0.0001, **p<0.01, *p<0.05.

See Table S1 for detailed Statistics.

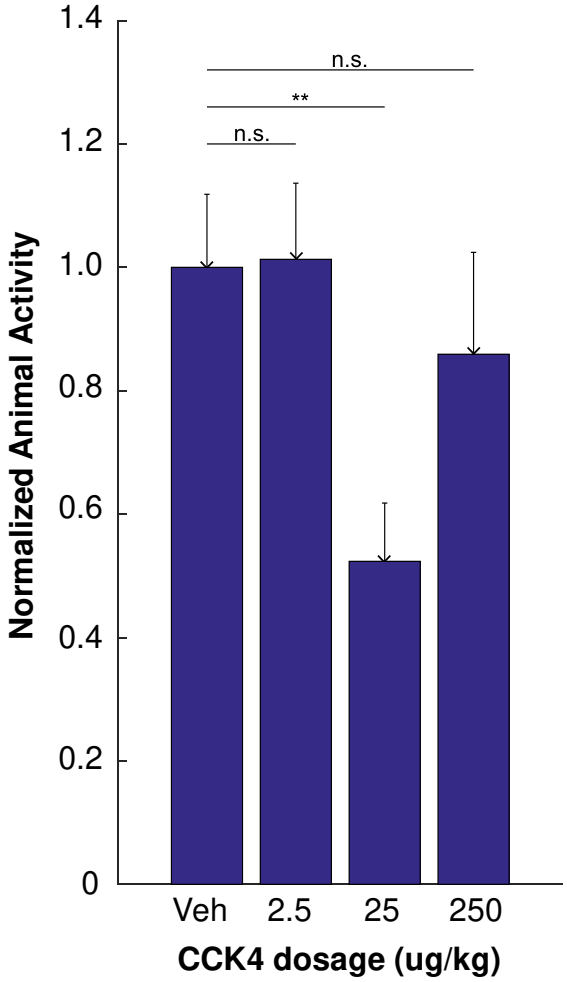

Supplementary Figure 5

Animal activities after different dosage of CCK4 injection. Data shows normalized activities of mice since 60 seconds after CCK4 or vehicle injection up until 180s. n = 10 for each group. **, $p<0.01$; n.s., not significant; one-way ANOVA.

Table S1. Statistics

Figure	Panel	Statistic test	Exact P-value, F-value with degree of freedom for ANOVAs, t-value with degree of freedom for t-test, n
1	D	Paired t-test	t=0.878, df=9, p=0.403, n=10
1	G and S1C	two-way RM ANOVA	Time*Manipulation F(1,27) = 25.125, p < 0.001; Adjustment: Bonferroni; CCK before vs after, p<0.001; ACSF before vs after, p=0.411; CCK before vs ACSF before, p=0.231; CCK after vs ACSF after, p<0.001; n=15 for ACSF group, n=14 for CCK group.
2	E to G	two-way RM ANOVA	Time*Manipulation F(1,21) = 10.49, p = 0.004; Adjustment: Bonferroni; HFLSEA before vs after, p<0.001; HFLSVA before vs after, p=0.623; HFLSEA before vs HFLSVA before, p=0.976; HFLSEA after vs HFLSVA after, p=0.005; n=13 for HFLSEA group, n=10 for HFLSVA group.
2	H to J	two-way RM ANOVA	Time*Manipulation F(1,16) = 9.711, p = 0.007; Adjustment: Bonferroni; HFLSEA before vs after, p=0.001; HFLSVA before vs after, p=0.898; HFLSEA before vs HFLSVA before, p=0.308; HFLSEA after vs HFLSVA after, p=0.006; n=8 for HFLSEA group, n=10 for HFLSVA group.
2	K to M	Paired t-test	t=-1.424, df=12, p=0.18, n=13
S2	D	Paired t-test	t=-0.899, df=8, p=0.395, n=9
3	G to I	two-way RM ANOVA	Time*Manipulation F(1,12) = 5.759, p =0.034; Adjustment: Bonferroni; HFLSEA before vs after, p=0.012; HFLSVA before vs after, p=0.67; HFLSEA before vs HFLSVA before, NA; HFLSEA after vs HFLSVA after, p=0.034; n=7 for HFLSEA group, n=7 for HFLSVA group.
3	J to L	two-way RM ANOVA	Time*Manipulation F(1,12) = 28.074, p <0.001; Adjustment: Bonferroni; HFLSEA before vs after, p<0.001; HFLSVA before vs after, p=0.814; HFLSEA before vs HFLSVA before, NA; HFLSEA after vs HFLSVA after, p<0.001; n=7 for HFLSEA group, n=7 for HFLSVA group.
4	E	unpaired t-test	t=1.964, df=539, p<0.001, n = 345 for EC, n = 199 for VC
S4		unpaired t-test	Animal 1: t=1.991, df=78, p <0.001, n=239 for EC, n=39 for VC; Animal 2: t=2.008, df=51, p=0.015, n=44 for EC, n=128 for VC; Animal 3: t=1.986, df=91, p=0.003, n=62 for EC, n=32 for VC.
			Time*Freq F(3,34)=10.666, p<0.001; Adjustment: Bonferroni.
			1Hz before vs after: p=0.352
			10Hz before vs after: p=0.044
			40Hz before vs after: p=0.003
			80Hz before vs after: p<0.001

5	A	two-way RM ANOVA	1Hz before vs 10Hz before	p=1
			1Hz before vs 40Hz before	p=1
			1Hz before vs 80Hz before	p=1
			10Hz before vs 40Hz before	p=1
			10Hz before vs 80Hz before	p=1
			40Hz before vs 80Hz before	p=1
			1Hz after vs 10Hz after	p=0.447
			1Hz after vs 40Hz after	p=0.052
			1Hz after vs 80Hz after	p<0.001
			10Hz after vs 40Hz after	p=1
			10Hz after vs 80Hz after	p=0.017
			40Hz after vs 80Hz after	p=0.208
			n=9, 8, 8, 13 for 1, 10, 40, 80 Hz, respectively	
5	B	two-way RM ANOVA	Time*Delay1 F(5,59)=7.115, p<0.001; Adjustment: Bonferroni.	
			minus65ms before vs after	p=0.945
			10ms before vs after	p<0.001
			85ms before vs after	p<0.001
			235ms before vs after	p<0.001
			535ms before vs after	p=0.003
			885ms before vs after	p=0.385
			minus65ms before vs 10ms before	p=1
			minus65ms before vs 85ms before	p=1
			minus65ms before vs 235ms before	p=1
			minus65ms before vs 535ms before	p=1
			minus65ms before vs 885ms before	p=1
			10ms before vs 85ms before	p=1
			10ms before vs 235ms before	p=1
			10ms before vs 535ms before	p=1
			10ms before vs 885ms before	p=1
			85ms before vs 235ms before	p=1
			85ms before vs 535ms before	p=1
			85ms before vs 885ms before	p=1
			235ms before vs 535ms before	p=1
			235ms before vs 885ms before	p=1
			535ms before vs 885ms before	p=1
			minus65ms after vs 10ms after	p<0.001
			minus65ms after vs 85ms after	p=0.001
			minus65ms after vs 235ms after	p=0.043
			minus65ms after vs 535ms after	p=0.457
			minus65ms after vs 885ms after	p=1
			10ms after vs 85ms after	p=1
			10ms after vs 235ms after	p=1
			10ms after vs 535ms after	p=0.443
			10ms after vs 885ms after	p=0.004
			85ms after vs 235ms after	p=1
			85ms after vs 535ms after	p=0.978
			85ms after vs 885ms after	p=0.012
			235ms after vs 535ms after	p=1
			235ms after vs 885ms after	p=0.221
			535ms after vs 885ms after	p=1
			n=13, 13, 13, 6, 10, 10 for Delay 1=-65, 10, 85, 235, 535, and 885 ms, respectively	

5	C	two-way RM ANOVA	Time*Delay2 F(5,51)=4.133, p=0.003; Adjustment: Bonferroni.	
			0ms before vs after	p<0.001
			50ms before vs after	p=0.001
			200ms before vs after	p=0.006
			400ms before vs after	p=0.073
			800ms before vs after	p=0.454
			∞ before vs after	p=0.363
			0ms before vs 50ms before	p=1
			0ms before vs 200ms before	p=1
			0ms before vs 400ms before	p=1
			0ms before vs 800ms before	p=1
			0ms before vs ∞ before	p=1
			50ms before vs 200ms before	p=1
			50ms before vs 400ms before	p=1
			50ms before vs 800ms before	p=1
			50ms before vs ∞ before	p=1
			200ms before vs 400ms before	p=0.497
			200ms before vs 800ms before	p=1
			200ms before vs ∞ before	p=1
			400ms before vs 800ms before	p=1
			400ms before vs ∞ before	p=1
			800ms before vs ∞ before	p=1
			0ms after vs 50ms after	p=0.374
			0ms after vs 200ms after	p=0.374
			0ms after vs 400ms after	p=0.074
			0ms after vs 800ms after	p=0.01
			0ms after vs ∞ after	p=0.006
			50ms after vs 200ms after	p=1
			50ms after vs 400ms after	p=1
			50ms after vs 800ms after	p=1
			50ms after vs ∞ after	p=1
			200ms after vs 400ms after	p=1
			200ms after vs 800ms after	p=1
			200ms after vs ∞ after	p=1
			400ms after vs 800ms after	p=1
			400ms after vs ∞ after	p=1
			800ms after vs ∞ after	p=1
			n = 13, 11, 12, 6, 6, 9 for Delay 2= 0, 50, 200, 400, 800 ms and ∞, respectively	
6	B	two-way RM ANOVA	Time*Manipulation F(3,45)=6.588, p=0.001; Adjustment: Bonferroni.	
			BaselineVS_ACSF vs PostVS_ACSF	p<0.001
			BaselineAS_ACSF vs PostAS_ACSF	p<0.001
			BaselineVS_ACSF vs BaselineAS_ACSF	p=1
			PostVS_ACSF vs PostAS_ACSF	p<0.001
			BaselineVS_L365260 vs PostVS_L365260	p=1
			BaselineAS_L365260 vs PostAS_L365260	p<0.001
			BaselineVS_L365260 vs BaselineAS_L365260	p=1
			PostVS_L365260 vs PostAS_L365260	p<0.001
			BaselineVS_ACSF vs BaselineVS_L365260	p=0.899
			BaselineAS_ACSF vs BaselineAS_L365260	p=0.678

			PostVS_ACSF vs PostVS_L365260	p<0.001
			PostAS_ACSF vs PostAS_L365260	p=0.962
			n=9 for ACSF group, n=8 for L360265 group	
6	D	two-way RM ANOVA	Time*Manipulation F(3,36)=17.631,, p<0.001; Adjustment: Bonferroni.	
			BaselineVS_Saline vs PostVS_Saline	p=1
			BaselineAS_Saline vs PostAS_Saline	p<0.001
			BaselineVS_Saline vs BaselineAS_Saline	p=1
			PostVS_Saline vs PostAS_Saline	p<0.001
			BaselineVS_CCK4 vs PostVS_CCK4	p<0.001
			BaselineAS_CCK4 vs PostAS_CCK4	p<0.001
			BaselineVS_CCK4 vs BaselineAS_CCK4	p=1
			PostVS_CCK4 vs PostAS_CCK4	p=0.01
			BaselineVS_Saline vs BaselineVS_CCK4	p=0.536
			BaselineAS_Saline vs BaselineAS_CCK4	p=0.792
			PostVS_Saline vs PostVS_CCK4	p<0.001
			PostAS_Saline vs PostAS_CCK4	p=0.264
			n=7 for CCK group, n=7 for Saline group	
6	E	one-way ANOVA	F(3,27)=28.797; posthoc Bonferroni test.	
			CCK4_CCKKO vs Saline_CCKKO	p<0.001
			CCK4_CCKKO vs L365260_C57	p<0.001
			CCK4_CCKKO vs ACSF_C57	p=0.002
			Saline_CCKKO vs L365260_C57	p=0.937
			Saline_CCKKO vs ACSF_C57	p=0.019
			L365260_C57 vs ACSF_C57	p<0.001
			n=7, 7, 8, 9 for CCK4_CCKKO, Saline_CCKKO, L365260_C57, and ACSF_C57, respectively	